Zhu, C., Pilz, M., Cotton, F. (2020): Which is a better proxy, site period or depth to bedrock, in modelling linear site response in addition to the average shear-wave velocity? - Bulletin of Earthquake Engineering, 18, 3, 797-820.

https://doi.org/10.1007/s10518-019-00738-6

Which is a better proxy, site period or depth to bedrock, in modelling linear site response in addition to the average shear-wave velocity?

Chuanbin Zhu[1] · Marco Pilz[1] · Fabrice Cotton[1,2]

Abstract

This study aims to identify the best-performing site characterization proxy alternative and complementary to the conventional 30 m average shear-wave velocity V_{S30}, as well as the optimal combination of proxies in characterizing linear site response. Investigated proxies include T_0 (site fundamental period obtained from earthquake horizontal-to-vertical spectral ratios), V_{Sz} (measured average shear-wave velocities to depth z, $z = 5$, 10, 20 and 30 m), $Z_{0.8}$ and $Z_{1.0}$ (measured site depths to layers having shear-wave velocity 0.8 and 1.0 km/s, respectively), as well as $Z_{x-infer}$ (inferred site depths from a regional velocity model, $x = 0.8$ and 1.0, 1.5 and 2.5 km/s). To evaluate the performance of a site proxy or a combination, a total of 1840 surface-borehole recordings is selected from KiK-net database. Site amplifications are derived using surface-to-borehole response-, Fourier- and cross-spectral ratio techniques and then are compared across approaches. Next, the efficacies of 7 single-proxies and 11 proxy-pairs are quantified based on the site-to-site standard deviation of amplification residuals of observation about prediction using the proxy or the pair. Our results show that T_0 is the best-performing single-proxy among T_0, $Z_{0.8}$, $Z_{1.0}$ and V_{Sz}. Meanwhile, T_0 is also the best-performing proxy among T_0, $Z_{0.8}$, $Z_{1.0}$ and $Z_{x-infer}$ complementary to V_{S3} in accounting for the residual amplification after V_{S30}-correction. Besides, T_0 alone can capture most of the site effects and should be utilized as the primary site indicator. Though (T_0, V_{S30}) is the best-performing proxy pair among (V_{S30}, T_0), (V_{S30}, $Z_{0.8}$), (V_{S3} , $Z_{1.0}$), (V_{S30}, $Z_{x-infer}$) and (T_0, V_{Sz}), it is only slightly better than ($T0$, V_{S20}). Considering both efficacy and engineering utility, the combination of T_0 (primary) and V_{S20} (secondary) is recommended. Further study is needed to test the performances of various proxies on sites in deep sedimentary basins.

Keywords

Site effects · Amplification · Site proxy · Surface-to-borehole spectral ratios · KiK-net · Earthquake

1 Introduction

An earthquake recording site was simply delineated as either rock or soil sites in some early ground-motion models (GMMs) (e.g., Si and Midoriakwa 1999) before being explicitly characterized according to a piecewise site classification scheme (e.g., Atkinson and Boore 2003) or, more recently, a continuous site proxy (e.g., Boore et al. 2014). Undoubtedly, the time-averaged shear-wave velocity in the first 30 m, V_{S30} (Borcherdt 1994) is the most widely used site or site class delineator.

However, many studies have shown that V_{S30} alone is not adequate to distinguish the site effects at one site from those at another (e.g., Gallipoli and Mucciarelli 2009; Kotha et al. 2018). Thus, efforts have been made in the search for alternative or complementary site proxies (or their combinations) to V_{S30}. Based on that site period T_0 is used for site classification in Japan for engineering design practice (Japan Road Association 1990). Zhao et al. (2006) proposed to utilize T_0 and horizontal-to-vertical (H/V) response spectral ratios over a wide period range to classify K-NET stations in Japan and

Electronic supplementary material. The online version of this article (https ://doi.org/10.1007/s10518-019-00738-6) contains supplementary material, which is available to authorized users.

✉ Chuanbin Zhu: chuanbin.zhu@gfz-potsdam.de

Extended author information available on the last page of the article

developed a GMM using the period-based classification scheme. Later, they found that T_0 was better than both V_{S30} for soft soil sites ($T_0 > 0.6$ s) at long periods (above 1.0 s), and for other site classes and spectral period bands, they performed equally well (Zhao and Xu 2013).

Cadet et al. (2012) compared the misfits of five single site proxies V_{Sz} (shear-wave velocity averaged to a depth z, $z = 5$, 10, 20, and 30 m) and T_0 and four site proxy pairs (T_0, V_{Sz}) in modelling KiK-net surface-to-borehole amplification. T_0 and (T_0, V_{S30}) were found to be the best single proxy and proxy pair, respectively. Régnier et al. (2014) concluded that, in addition to V_{S30}, T_0 could reduce the site-to-site amplification variability of KiK-net sites in deep sedimentary basins within a specific V_{S30} class. Applying neural network approach to KiK-net data, Derras et al. (2017) considered V_{S30} and T_0 to be the best single-proxy for periods below and above 0.6 s, respectively.

Outside Japan, McVerry (2011) reported that, in New Zealand, site effects could be better characterized using T_0 than using V_{S3} for oscillator periods of 0.5 s or longer. Hassani and Atkinson (2018a) concluded that T_0 was better than V_{S30} in parameterizing sites in Central and Eastern North America. Meanwhile, for sites in California, Hassani and Atkinson (2018b) achieved an average 5% further reduction in the standard deviation of residuals by including T_0 after accounting for the site effects associated with V_{S30} and $Z_{1.0}$ (depth to $V_S = 1.0$ km/s). For recording stations in Italy, Luzi et al. (2011) realized a significant reduction in standard deviation when V_{S30} and T_0 are used together compared to a V_{S30}-based site classification. In addition to the empirical investigation, Stambouli et al. (2017) utilized the proxy pair (V_{S3} , T_0) to model numerical site responses of hundreds of global soil columns and achieved a reduction in intersite variance by over 60% compared to a model without site term.

Several previous research (e.g., Zhao and Xu 2013) focus on searching for a better alternative to V_{S30}. However, the period-dependency of site amplification determines that there is no such a single proxy that performs the best for all oscillator periods. Thus, to improve the site amplification estimation over the whole period range of engineering interest, it is more viable to use a combination of site proxies than to use a single predictor variable. Meanwhile, the efforts devoted to measuring or inferring V_{S30} in the past decades, as well as the established status of V_{S30} in current seismic regulations render the idea of replacing V_{S30} unappealing. Therefore, to reduce the uncertainty associated with site characterization, it is deemed practical to find an additional site proxy to characterize the site effects that cannot be depicted by V_{S30} alone, namely an easy-to-measure site proxy complementary to V_{S30}.

Site period T_0, as well as site depths $Z_{0.8}$ and $Z_{1.0}$, are all potential additional parameters, where $Z_{0.8}$ and $Z_{1.0}$ are the depths in meters to isosurfaces having shear-wave velocities 0.8 and 1.0 km/s, respectively. Then the question arises as to which parameter, is the most suitable proxy secondary to V_{S30} in modelling site response. T_0 can be reliably obtained for many sites at relatively low costs using the horizontal-to-vertical (H/V) spectral ratio ($HVSR$) technique (Nakamura 1989; Lermo and Chávez-García 1993) and thus was proposed by Pitilakis et al. (2004, 2013, 2018) as a parameter for site classification specifically in Eurocode 8. However, the NGA-West2 GMMs (e.g., Boore et al. 2014, hereafter referred to as BSSA14) chose site depth as the secondary proxy, but there is no unanimous answer as to which depth parameters should be utilized. For instance, the revised European building code Eurocode 8 proposes to include $Z_{0.8}$, but BSSA14 opted for $Z_{1.0}$ in their site terms.

Therefore, we dedicate this article in search of the best-performing site proxies not only alternative but also complementary to V_{S30} in characterizing linear site response. We will first present the KiK-net dataset used in this study, including site data and ground-motion data. Then we will describe different techniques utilized in this investigation, including response-, Fourier- and cross-spectral ratio approaches, to evaluate site effects and then compare the site amplifications (AF) derived using these methods. This is followed by residual analyses in which site amplification is modelled as a

function of various site proxies or their combinations. The performance of a site proxy or a combination is gauged based on the standard deviation of residuals between the observed amplification and the amplification predicted from the proxy or the combination.

2 Data selection

We use a KiK-net database which consists of about 157,000 ground-motion time-series recorded between October 1997 and December 2011. These records were processed by Dawood et al. (2016) following a stringent fully-automated processing protocol. Data processing was elaborated by Dawood et al. (2016), and thus we only briefly introduce the procedure.

Time-series were firstly baseline corrected, tapered and zero-padded. Then, a high-pass corner frequency f_c (0.04 Hz) was pre-selected to filter a record (three components for the surface station and three for the borehole station) using a high-pass, acausal, fourth-order Butterworth filter. The selection of f_c would then be confirmed if the filtered records passed the check on its final displacement, the ratio between the final and the maximum displacements, the slope of the trailing portion of the displacement and velocity time-histories, as well as the trend of the smoothed Fourier amplitude spectrum. Otherwise, the above filter process would be iterated using a higher f_c until a suitable f_c was found. Then, each component was checked on its signal-to-noise ratio (SNR ≥ 3) in the frequency range between $2f_c$ and 30 Hz and was flagged whether it passed the signal-to-noise ratio check or not. For more details about data processing, readers are encouraged to refer to Dawood et al. (2016).

From the processed database, we select ground motions with rupture distance (R_{rup}) up to 400 km, with f_c no lower than 0.12 Hz, passing the signal-to-noise ratio (SNR ≥ 3) check and from earthquakes with a moment magnitude (M_w) between 3.0 and 8.0. Thus, all selected records have a maximum usage period of at least $1/(2f_c) = 4.17$ s. There are certain correlations between some parameters, e.g., short-period rock site spectral amplitude to source distance, and long-period rock site spectral amplitude to earthquake magnitude. However, magnitude and source distance exerted little influence on site amplification if the effect of nonlinear response was represented by using a function of rock site spectral values (Bazzurro and Cornell 2004). Thus, within the linear domain, site effects are often treated to be independent of earthquake magnitude and source-site distance in GMMs.

Therefore, to minimize the potential influences of magnitude and distance on site response, we limit our research on linear amplification. This is achieved by further selecting ground motions that are not significantly affected by soil nonlinearity based on its shear strain. Fujimoto and Midorikawa (2006) defined the minimum level of shear strain for a possible nonlinear response to be 3×10^{-4}. The maximum shear strain within a velocity profile can be estimated using:

$$y'_{eff} = 0.4PGV/V_{S30} \quad (1)$$

where y'_{eff} is the maximum shear strain at a recording site, and PGV is the peak ground velocity (m/s). Ground motions with y'_{eff} exceeding 3×10^{-4} are excluded from our dataset (Fig. 1a). Thus, we can assume a linear site response in this study.

In this study, site amplification at a surface station is referenced to its borehole sensor which is situated in layers at different depths and with various shear-wave velocities for different stations (Fig. 1b). To minimize the influence of inhomogeneous reference site condition on surface-to-borehole spectral ratios, we only utilize KiK-net sites with a shear-wave velocity at borehole ($V_{S,hole}$)

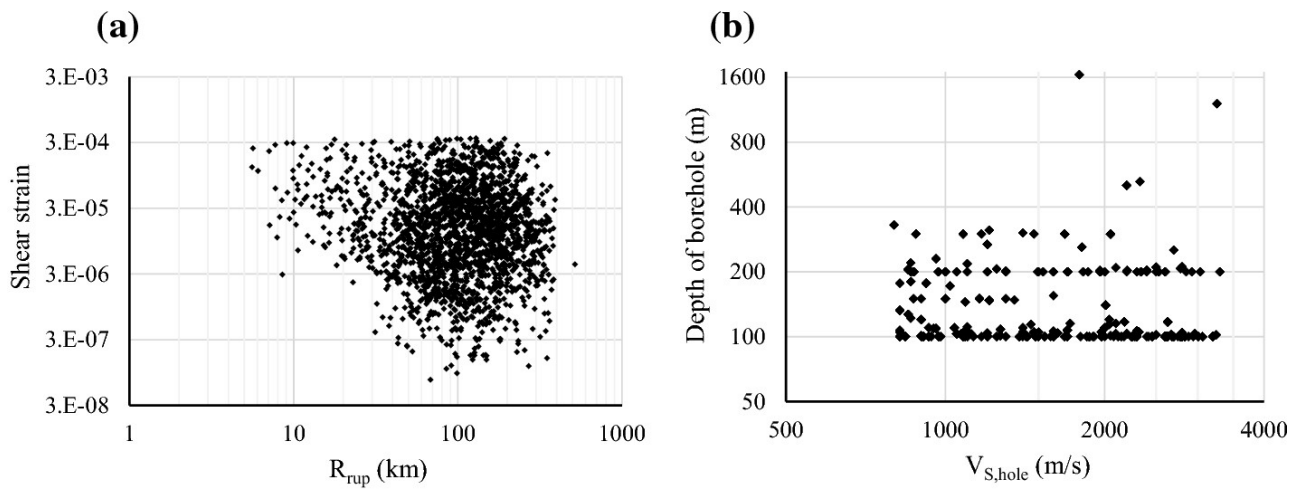

Figure 1. *(**a**) Nonlinearity check; and (**b**) site conditions of borehole stations.*

above 800 m/s (Régnier et al. 2014). As shown in Fig. 1b, selected recording stations have $V_{S,hole}$ in the range between 800 and 3300 m/s and are at least 100 m below the ground surface. As demonstrated by Oth et al. (2011), only a few KiK-net velocity profiles have an abrupt velocity contrast below the depth of 100 m, and on average site effects of velocity structures deeper than 100 m are insignificant. Thus, we do not correct the borehole records to a common depth.

For a site with multiple recordings, its intra-site (within-site) amplification variability can be partially attributed to the lateral inhomogeneity of near- and/or sub-surface velocity structures, thus, we only use stations that recorded at least three seismic events. The surface-to-borehole spectral ratios are then averaged over all records at a site to minimize the intra-site variability associated with the azimuthal effects of incoming waves on site response (Field et al. 1992). Then the deviation of the observed amplification at a specific site from the median amplification predicted using site proxy or proxies is treated as the site-to-site (inter-site) residual which arises from the inadequacy of site proxy or proxies, e.g., V_{S30}, (V_{S30}, T_0) or (V_{S30}, $Z_{0.8}$), in characterizing a site (e.g., Al Atik et al. 2010). The standard deviation of amplification residuals is taken as the inter-site standard deviation, which represents site-to-site amplification variability.

Though inter-site and intra-site residuals can be partitioned using a mixed-effect model (Abrahamson and Youngs 1992), we do not adopt this approach herein for two reasons. Firstly, the inter-site and intra-site residuals cannot be completely separated from each other even when a mixed-effect model is used (Zhao and Xu 2013). More importantly, the purpose of this study is to evaluate the performances of various site proxies in modelling site effects, and a good proxy or proxy combination is supposed to reduce both the total and inter-site variabilities, as shown by Derras et al. (2017). Therefore, a stringent partition between inter-and intra-site standard deviation is not implemented in this study.

Finally, there are 1840 ground motions selected in this study. The distribution of selected records is presented in M_w-R_{rup} space in Fig. 2a, and the number of recordings at each period and at each station is illustrated in Fig. 2b and c, respectively. Average velocities (V_{Sz}) and site depths ($Z_{0.8}$ and $Z_{1.0}$) of recording stations are derived from available one-dimensional (1D) velocity profiles which are established from downhole PS-logging (Aoi et al. 2000; Okada et al. 2004). Though these PS-logging data might be unreliable at some sites (Kawase and Matsuo 2004; Pilz and Cotton 2019), they are the best information publicly available at this stage.

Wang et al. (2018) derived fundamental periods (T_0) of KiK-net sites using the horizontal-to-

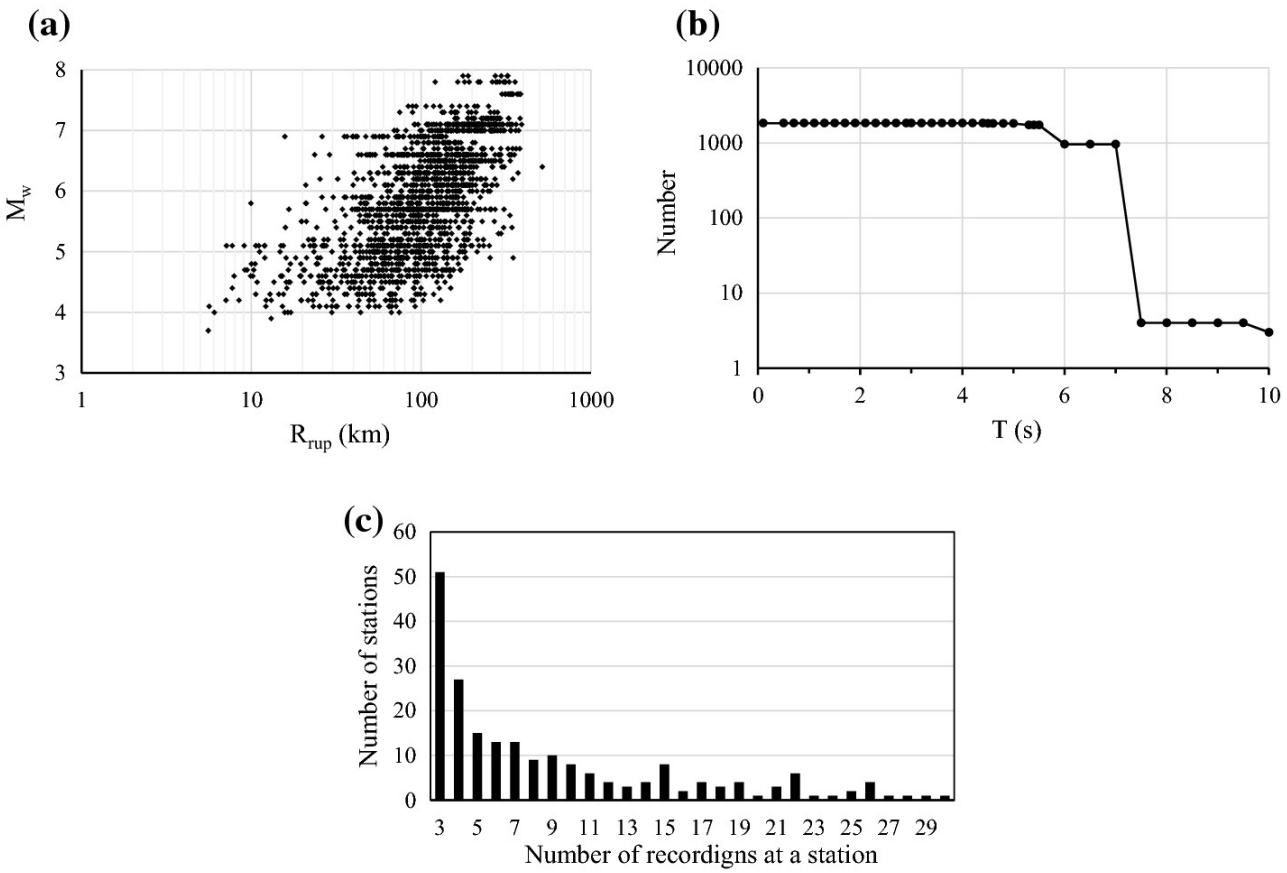

Figure 2. *Selected ground motions (**a**) M_w versus R_{rup}; (**b**) number of recordings at each period; and (**c**) number of recordings per station.*

vertical spectral ratio ($HVSR$) technique. Individual $HVSR$ curve was computed on 5%-damped response spectrum of earthquake ground motions (complete waveforms) and then was averaged over all recordings (at least 10) at a given site. Local maximum points on an average $HVSR$ curve with amplitudes larger than both $1.48 * \overline{HVSR}$ and 2.0 were considered as significant peaks, where $HVSR$ is the average $HVSR$ curve integrated over all usable periods. For sites with more than one significant peak, the longest period peak was taken as the fundamental mode and its period as T_0. However, T_0 was only assigned to a site if it passed a consistency-check, namely $0.5 < T_0/T_R < 2.0$, where T_R is the theoretical fundamental period calculated from a velocity profile using the Rayleigh method (Biggs 1964). Site fundamental periods derived by Wang et al. (2018) are utilized in this study.

All site parameters used in this investigation, including V_{Sz}, T_0, $Z_{0.8}$ and $Z_{1.0}$, are obtained from site-specific measurements. The distributions of V_{S30} against $Z_{0.8}$ and $Z_{1.0}$are illustrated in Fig. 3. T_0 is correlated with $Z_{0.8}$ and $Z_{1.0}$ to different extents. T_0 is depicted against V_{Sz} in Fig. 4, which shows that there are a few sites with T_0 larger than 1.0 s. The 5th, 50th and 95th percentile values of site data are also given in Table 1.

3 Surface-to-borehole spectral ratios

3.1 Fourier spectral ratio (SSRFAS)

In the frequency domain, amplitude spectrum $A_{ki}(f)$ of a recording at a surface site (i) during an earthquake (k) can be represented by the convolution of the source, path and site effects:

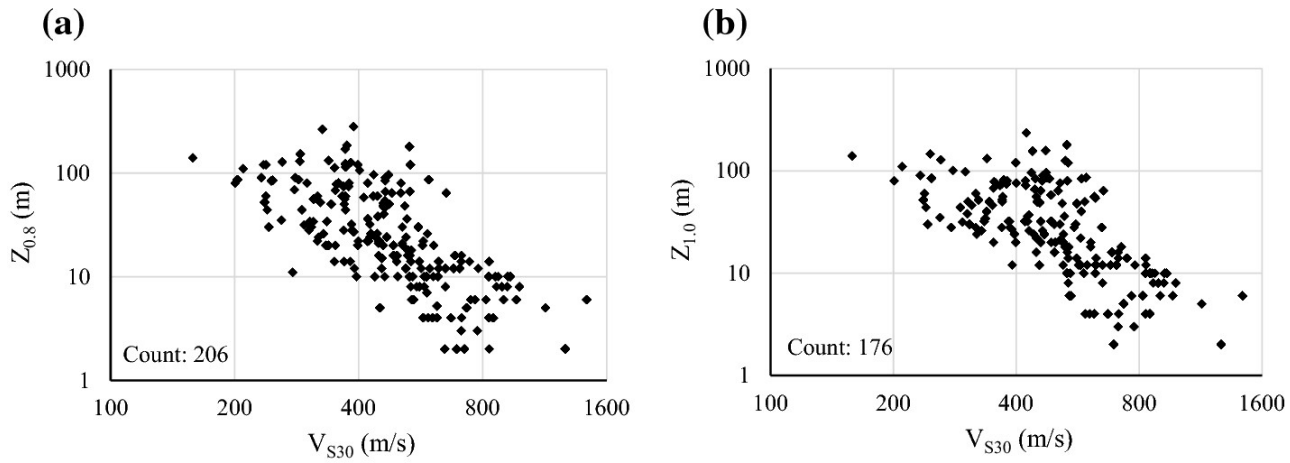

*Figure 3. Selected KiK-net recording stations (**a**) V_{S30} vs. $Z_{0.8}$; (**b**) V_{S30} versus $Z_{0.8}$.*

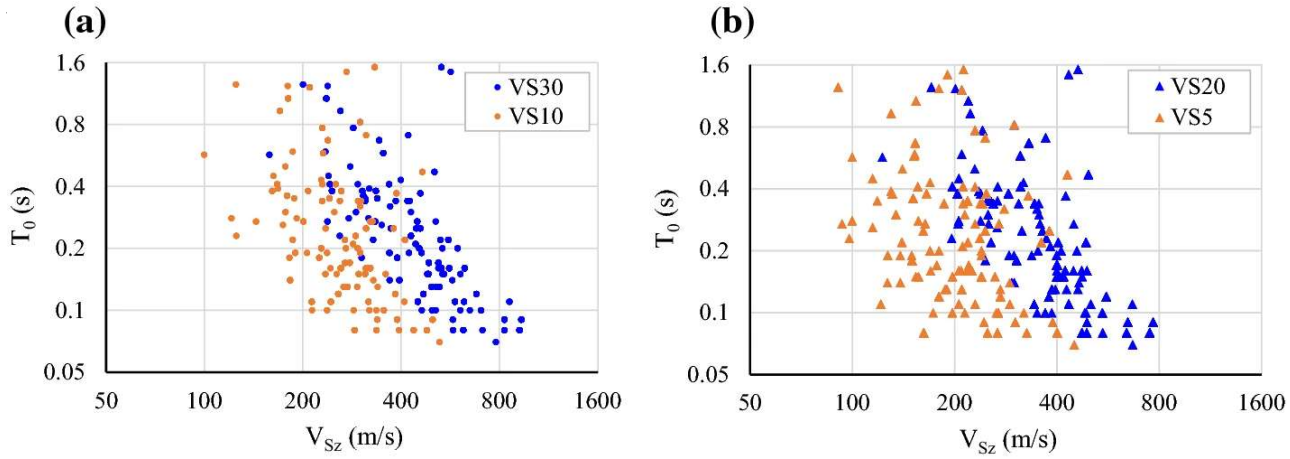

*Figure 4. Selected KiK-net recording stations (**a**) V_{S10} and V_{S30} versus T_0; (**b**) V_{S20} and V_{S5} versus T_0.*

$$A_{ki}(f) = O_k(f) \cdot P_{ki}(f) \cdot S_i(f) \tag{2}$$

where $O_k(f)$ is the source term of event k; $P_{ki}(f)$ is the path term between station i and event k; and $S_i(f)$ is the site term for station i.

Standard spectral ratio (SSR) technique is to calculate the ratio of the Fourier amplitude spectrum (FAS) of a recording at a site of interest (i) to that at a reference site (j). If the reference site has similar source and path effects to the site of interest and has negligible site response (ideally a flat transfer function with an amplitude of one), the spectral ratio is an estimate of site response at site i. Then the SSRFAS of the recording at the station (i) to that at the reference station (j) can be simplified as follows:

$$SSR_{k,ij}(f) = \frac{A_{k,i}(f)}{A_{k,j}(f)} = \frac{O_k(f) \cdot P_{k,i}(f) \cdot S_i(f)}{O_k(f) \cdot P_{k,j}(f) \cdot S_j(f)} = \frac{S_i(f)}{S_j(f)} \approx S_i(f) \tag{3}$$

Table 1
Percentile values of site data

Percentile	V_{S5} m/s	V_{S10} m/s	V_{S20} m/s	V_{S30} m/s	$Z_{0.8}$ m	$Z_{1.0}$ m	T_0 s
5th	119	165	206	241	4	4	0.08
50th	220	291	396	465	22	28	0.22
95th	477	569	761	897	127	126	1.20

3.2 Response spectral ratio (SSRPSA)

SSR is conventionally calculated using FAS of an earthquake recording. However, response spectrum or pseudo-spectral acceleration (PSA) has also been used by some researchers (e.g., Zhao et al. 2006; Cadet et al. 2012) due to some of its merits. Firstly, response spectral amplitude reflects structural response (a series of oscillators of varying natural frequency) and thus is widely adopted in engineering-orientated research, although Fourier spectrum has an explicit physical meaning. In addition, the Fourier spectrum requires extra soothing to reduce the effects of noise on spectral ratios (Safak 1997). In contrast, the damping ratio (e.g., 5%) of the response spectrum has a uniform smoothing effect on all recordings (Zhao et al. 2006).

Cadet (2007) calculated spectral ratios of KiK-net sites using both FAS and PSA. They found that, in a statistical sense, the SSR_{PSA} was comparable to SSR_{FAS} in the period range between 0.07 and 2.0 s but was higher than SSR_{FAS} outside this range. However, Safak (1997) reported that SSR_{PSA} was only comparable to SSR_{FAS} at long periods (>~1.0 s) but were higher than SSR_{FAS} at other frequencies. Given the conflicting results, both SSR_{PSA} and SSR_{FAS} are obtained for a surface-borehole station pair in this study.

3.3 Cross-spectral ratio (c-SSR_{FAS})

SSR approach should be implemented with caution when the reference site is in a borehole rather than on surface-rock. This is because the downhole recording usually contains downgoing waves reflected from the free surface and other interfaces between sedimentary layers, as well as waves scattered from local inhomogeneity (e.g., Shearer and Orcutt 1987). These downgoing waves can interfere destructively with the upgoing incident waves at some frequencies, producing a notch in the FAS of the borehole recording and thus artificial peaks in surface-to-borehole spectral ratios (e.g., Steidl 1993).

Cross-spectral ratio (c-SSR) is defined as the product of the spectral ratio estimate and the coherence function (Eqs. 4, 5), implicitly accounting for the record coherence in the formulation of site response estimate (e.g., Bendat and Piersol 1980). Thus, the c-SSR technique is recommended for surface-borehole recordings (Steidl 1993; Safak 1997; Assimaki et al. 2008). Since recording stations with $V_{S,hole} < 800$ m/s are excluded in this study, effects of downgoing waves on borehole recordings can be minimized but cannot be ruled out completely. Hence, the c-SSR approach is also implemented in this study.

$$c - SSR_{xy}(f) = \frac{P_{xy}(f)}{P_{xx}(f)} \tag{4}$$

$$C_{xy}(f) = \frac{\left|P_{xy}(f)\right|^2}{P_{xx}(f)P_{yy}(f)} \tag{5}$$

in which $P_{xx}(f)$ and $P_{yy}(f)$ are the power spectral densities of the surface (x) and borehole (y) recordings, respectively; $P_{xy}(f)$ is the cross power spectral densities between x and y; $C_{xy}(f)$ is the magnitude-squared coherence, which is a function of frequency with values ranging between 0 and 1.

All three techniques, including SSR_{PSA}, SSR_{FAS} and c-SSR_{FAS}, are utilized to derive surface-to-borehole spectral ratios in this study. SSR_{PSA} at each horizontal component is computed as the ratio of 5% damped pseudo-spectral acceleration of the waveform recorded at the ground surface to that recorded at the borehole. The geometrical mean of the SSR_{PSA} in each horizontal direction is used and then averaged over different events (≥ 3) recorded at the site. SSR_{FAS} and c-SSR_{FAS} are obtained in a

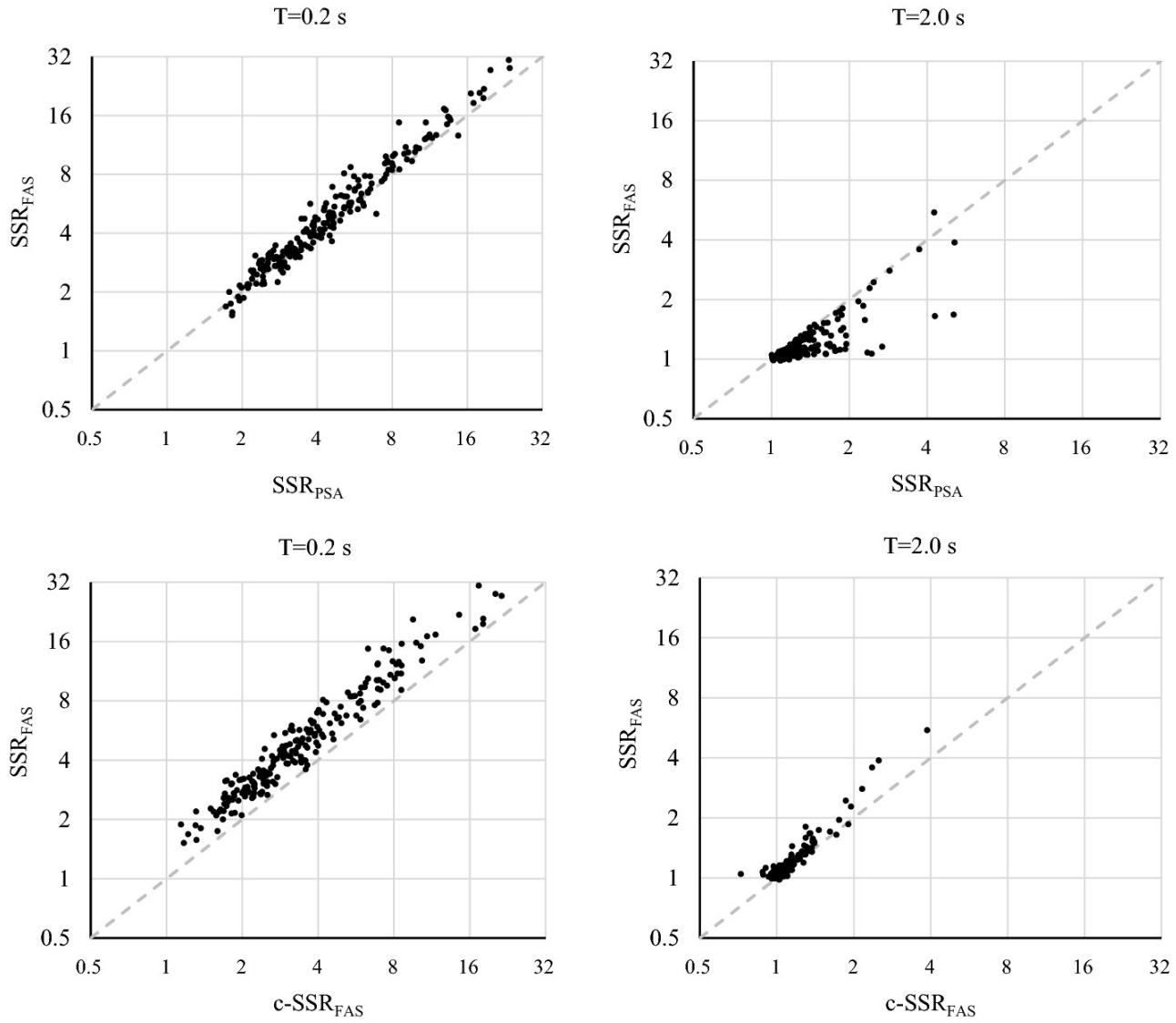

Figure 5. *Comparison between SSR_{PSA}, SSR_{FAS} and c-SSR_{FAS} at 0.2 (first column) and 2.0 s (second column).*

similar manner to SSR_{PSA}. One difference lies in that SSR_{FAS} is calculated as the ratio of FAS between surface and borehole recordings, while c-SSR_{FAS} is derived as the ratio of the cross-power density spectrum between the surface and downhole recordings to the power density spectrum of surface recording using Welch's method (Welch 1967). The other difference is that, for SSR_{FAS} and c-SSR_{FAS}, we take an extra step - smoothing before deriving the spectral ratio. Konno and Ohmachi (Konno and Ohmachi 1998) smoothing is utilized with a bandwidth coefficient $b = 20$.

3.4 Comparison of SSR_{PSA}, SSR_{FAS}, and c-SSR_{FAS}

Values of SSR_{FAS} are compared with those of SSR_{PSA} and c-SSR_{FAS} at $T = 0.2$ and 2.0 s in Fig. 5. SSR_{FAS}s, SSR_{PSA}s and c-SSR_{FAS}s at different spectral periods are given in Online Resource 1. It is worth noting that, in Fig. 5, amplifications at $T = 2.0$ s are much less notable than at $T = 0.2$ s. This is because that most selected KiK-net sites do not have very thick sediments. There are only 20 (or 10%) sites with $Z_{0.8}$ more than 100 m (Fig. 3) and also a few sites with T_0 above 1.0 s (Fig. 4). Thus, at these investigated KiK-net stations, site effects are not significant at relatively long periods (>~1.0 s).

Ratios between SSR_{PSA} and SSR_{FAS}, as well as between c-SSR_{FAS} and SSR_{FAS} at various periods are

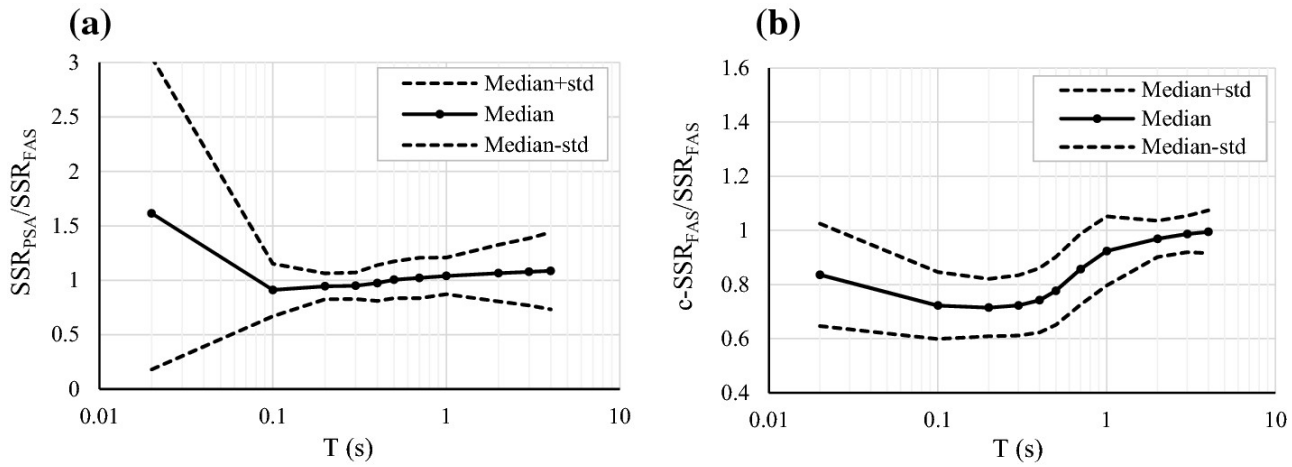

Figure 6. *Ratios of (**a**) SSR_{PSA} to SSR_{FAS} and (**b**) c-SSR_{FAS} to SSR_{FAS} at various spectral periods.*

presented in Fig. 6. At $T = 0.02$ s, SSR_{PSA} deviates significantly from SSR_{FAS} (Fig. 6a). This is attributable to the peculiarity of response spectrum of which spectral content is not directly proportional to that of the corresponding Fourier spectrum at some oscillator periods (or frequencies). For instance, peak ground acceleration (PGA) is controlled by the entire Fourier spectrum (e.g., Bora et al. 2016). In addition, the strong scenario-dependency of response spectral ratios at short periods (Stafford et al. 2017) may explain the large scatter at $T = 0.02$ s in Fig. 6a. However, at $T = 0.2$ s, SSR_{PSA} is, on average, only slightly smaller than SSR_{FAS} with $SSR_{PSA}/SSR_{FAS} = 0.94$ ($\pm$ 0.12) (Fig. 6a), and then the ratio between SSR_{PSA} and SSR_{FAS} increases gradually with the oscillator period, reaching 1.09 ($\pm$ 0.35) at $T = 4.0$ s, suggesting an insubstantial divergence in the period range between 0.2 and 4.0 s. The trend of SSR_{PSA}/SSR_{FAS} with period (Fig. 6a) is compatible with the results of Cadet (2007). In Fig. 6b, the median value of c-SSR_{FAS}/SSR_{FAS} is systematically lower than unity in the period range from 0.1 to 4.0 s. For instance, the ratio between c-SSR_{FAS} and SSR_{FAS} is 0.71 ($\pm$ 0.11) at $T = 0.2$ s. As pointed out by many researchers (e.g., Field et al. 1992; Steidl 1993), c-SSR does give a consistently lower amplification than SSR.

As indicated by Assimaki et al. (2008) and Thompson et al. (2009), downgoing waves could be identified in KiK-net recordings but did not severely contaminate the borehole records. This is especially true for our KiK-net dataset because of the inclusion of only sites with $V_{S,hole} \geq 800$ m/s. For these sites, abrupt velocity contrasts are more likely to be present above borehole sensors, resulting in the trapping of seismic waves between a velocity contrast and the free surface and thus inhibiting the surface reflections reaching downhole stations (e.g., Oth et al. 2011). However, destructive interferences at downhole stations, though deemed insubstantial here, still cannot be completely excluded and may contribute to the upward bias in SSR_{FAS}. This is evidenced by the shrinking aberration with the increase in spectral periods. Since for most selected KiK-net sites, $T_{S,ave}$ at which fundamental mode of destructive interference between incident waves and surface reflections occurs is below 1.0 s (85th percentile), as shown in Fig. 7, constructive interference has a negligible impact on the selected dataset at spectral periods above 1.0 s, e.g., c-SSR_{FAS}/SSR_{FAS} = 0.97 ($\pm$ 0.07) at $T = 2.0$ s and 0.99 ($\pm$ 0.08) at $T = 4.0$ s (Fig. 6b).

Another reason for the deviation between SSR_{FAS} and c-SSR_{FAS} is that noises in signals have different impacts on them. For noise-free data, SSR_{FAS} is identical to c-SSR_{FAS}. If noise is present in recordings, it will modify the SSR_{FAS} and c-SSR_{FAS} by factors $[(1 + SNR_S^{-2})/(1 + SNR_B^{-2})]^{0.5}$ and $1/(1 + SNR_B^{-2})$, respectively, where SNR_S and SNR_B represent signal-to-noise ratios of surface and borehole recordings, respectively. There is relatively little noise in downhole recordings compared with those

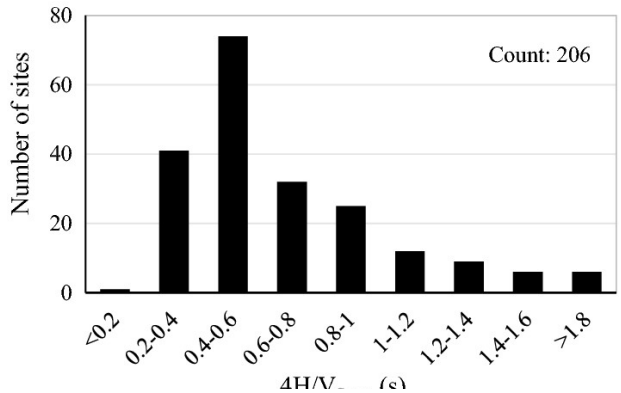

Figure 7. *Fundamental period of constructive interference between up-and down-going seismic waves at a borehole station. $T_{S,ave} = 4H_{Hole}/V_{S,hol}$, in which H_{Hole} is the distance and time-averaged velocity between the ground surface and downhole sensors.*

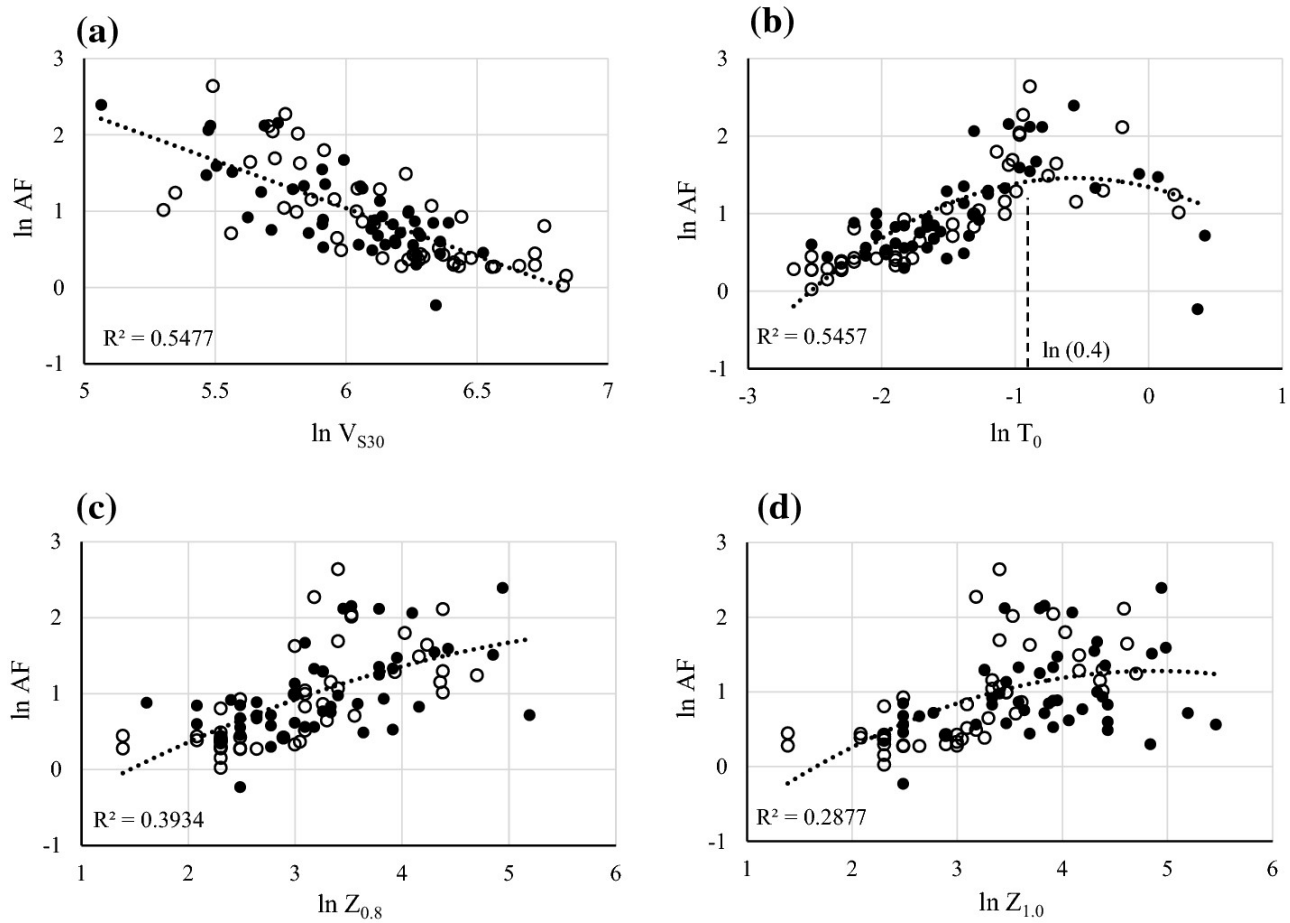

Figure 8. *Site amplification (c-SSR$_{FAS}$) at $T = 0.4$ s versus **(a)** V_{S30}, **(b)** T_0, **(c)** $Z_{0.8}$, and **(d)** $Z_{1.0}$ in ln–ln space. Dots represent sites with $800 < V_{s,hole} < 1800$ m/s whereas circles are sites with $1800 < V_{s,hole} < 3300$ m/s. The dotted line in each plot represents the regression to all data points, and R2 is the coefficient of determination.*

at the ground surface (Field et al. 1992), thus SSR$_{FAS}$ will be scaled up whereas c-SSR$_{FAS}$ will remain relatively unchanged.

4 Site proxies alternative to V_{S30}

After obtaining site amplifications using SSR$_{PSA}$, SSR$_{FAS}$ and c-SSR$_{FAS}$ (Online Resource 1), we first model the observed amplification factor (AF) at a given spectral period using a single site proxy, i.e., V_{Sz}, T_0, $Z_{0.8}$ and $Z_{1.0}$. Fig 8a–c depicts the AF at $T = 0.4$ s derived using c-SSR$_{FAS}$ against V_{S30}, T_0, $Z_{0.8}$ and $Z_{1.0}$, respectively. AF decreases with the increase in V_{S30} at $T = 0.4$ s (Fig. 8a) and all other

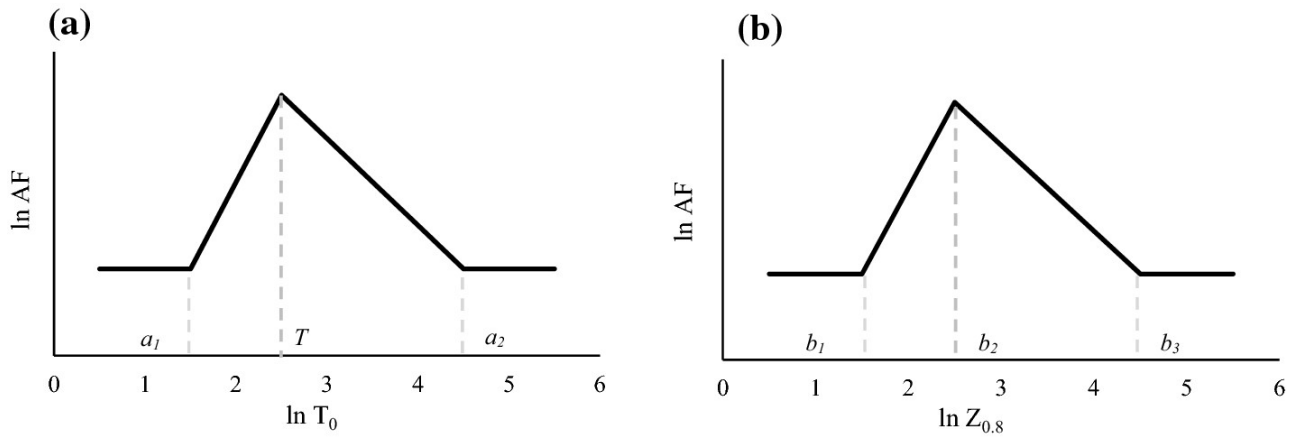

Figure 9. *Trends of amplification with* ***(a)*** T_0 *and* ***(b)*** $Z_{0.8}$ *(or* $Z_{1.0}$*) at a given spectral period.*

spectral periods except for 0.02 and 0.1 s at which AF scales positively with V_{S30}. Kawase and Matsuo (2004) also found an increase of AF with V_{S30} at very short periods (e.g., 0.06 and 0.08 s) using K-NET, KiK-net and JMA stations.

For a simple configuration of layered sediments underlain by bedrock, surface-to-bedrock amplification is governed by two competing phenomena, impedance contrast and attenuation (e.g., intrinsic material damping, geometric spreading and scattering). The increase of AF with V_{S30} at short periods may be caused by the fact that the detrimental impact of short-period (high-frequency) attenuation (e.g., Van Houtte, et al. 2011) on amplification outweigh the incremental effect of impedance contrast. For a site with a large V_{S30}, high-frequency wave energies tend to be attenuated to a lesser extent than they are at a softer site, resulting in a higher AF at a stiffer site.

In the linear range, many amplification models or site terms in GMMs (e.g., BSSA14) introduce a limiting velocity beyond which amplification no longer scales with V_{S3} . This limiting velocity (V_c in BSSA14) is period-dependent and decreases with the spectral period. For example, the value of limiting velocity V_c in BSSA14 is as large as 1500 m/s at 0.02 s, reducing to 844 m/s at 4.0 s. Since only a few sites investigated in this study have a V_{S30} higher than 800 m/s (Fig. 3), a limiting velocity is considered unnecessary in this research, and a simple linear function Eq. 6 is used for V_{S30}. However, as shown in Fig. 8b–d, AF does not scale linearly with T_0, $Z_{0.8}$ and $Z_{1.0}$. The relationships of AF with site period and depth can be represented by a piecewise linear function, as shown in Fig. 9a and b, respectively. Hassani and Atkinson (2018a, b) modelled the trend of AF with T_0 using a similar function as shown in Fig. 9a and fixed a_1 and a_2 to 0.05 and 2.0 s, respectively. However, our results show that all these coefficients (e.g., a_1 and b_1) are period-dependent. With current dataset, it is difficult to constraint all these period-dependent coefficients.

However, based on visual inspection, the relationship between AF and T_0 can also be described by a polynomial function. Given the purpose of the present research is to evaluate the efficacy of site proxies, rather than proposing a robust AF estimation model, we thus depict the trend using a polynomial function. The function with fewest terms that are statistically significant is a quadratic function. Hence a second-order polynomial (Eq. 7) is adopted to characterize the variations of AF with T_0, $Z_{0.8}$ and $Z_{1.0}$. We calculate the amplification residual Res_1 (Eq. 8) of observation about the regression line (Eqs. 6 or 7), as well as the standard deviation of amplification residuals σ_{Res1} according to Eq. 9. The performance of each site parameter is assessed based on σ_{Res1}, which is displayed in Fig. 10 for each amplification model using a single proxy.

$$\ln[AF(V_{S30})] = a_0 + a_1 \ln(V_{S30}) \tag{6}$$

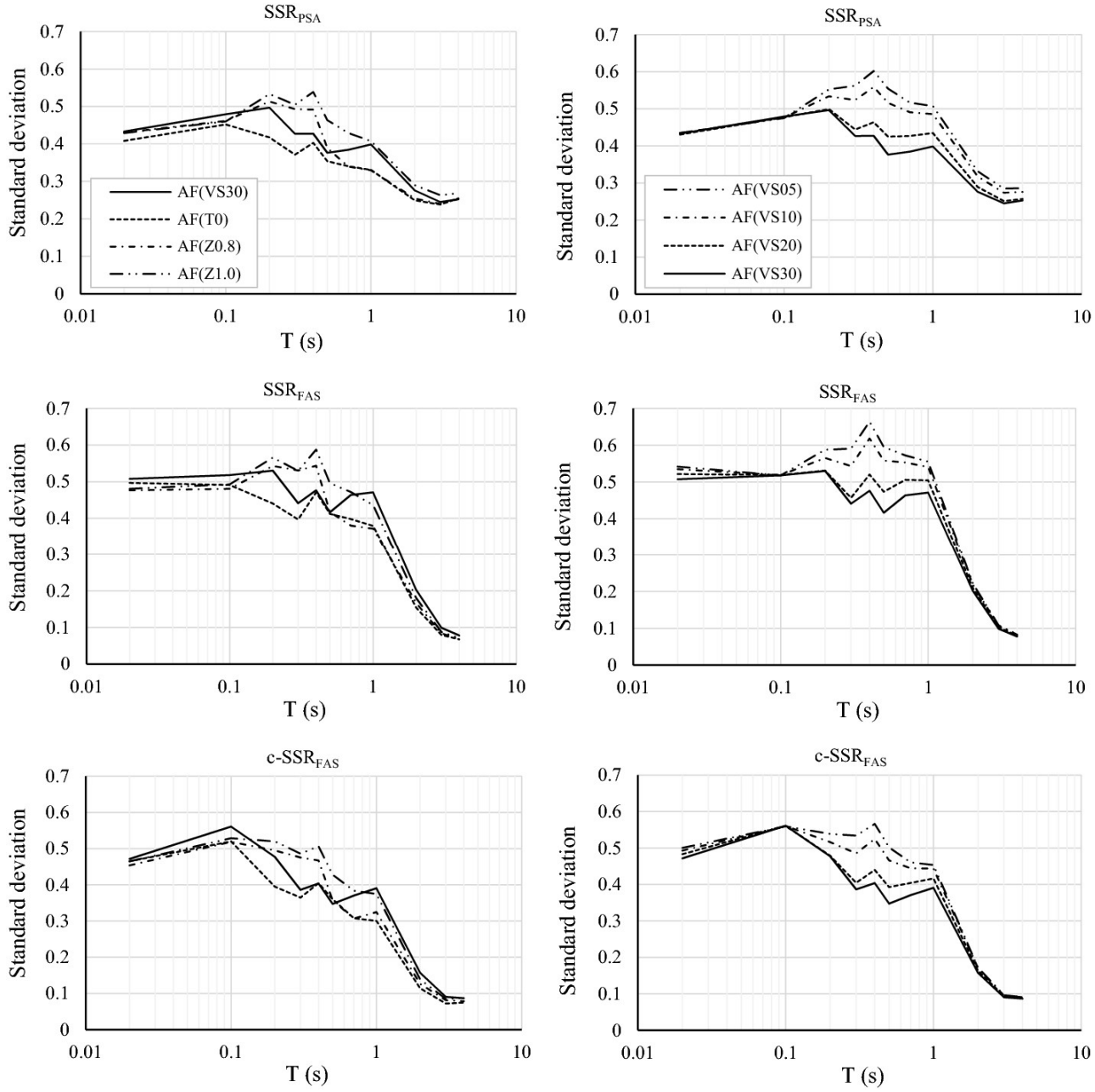

Figure 10. *Standard deviations of intersite amplification residuals of AF models using a single site proxy.*

$$\ln[AF(Y)] = b_0 + b_1 \ln(Y) + b_2[\ln(Y)]^2 \tag{7}$$

$$Res_1 = \ln(AF_{obs}) - \ln(AF_{pre}) \tag{8}$$

$$\sigma_{Res1} = \sqrt{\frac{\sum_1^N [\ln(AF_{obs}) - \ln(AF_{pre})]^2}{N}} \tag{9}$$

where AF_{obs} - Observed site amplification at a certain period using either SSR_{PSA}, SSR_{FAS} or $c\text{-}SSR_{FAS}$; AF_{pre} - Predicted site amplification, including $AF(V_{S3})$ and $AF(Y)$; $AF(V_{S30})$ and $AF(Y)$ - Site

amplifications predicted using V_{S3} and Y, respectively; Y - Site period or depths, e.g., T_0, $Z_{0.8}$ or $Z_{1.0}$; Res_1 - Amplification residual; σ - Standard deviation of amplification residuals; N - Number of sites.

Figure 10 shows that, among V_{S30}, T_0, $Z_{0.8}$ and $Z_{1.0}$, there is no one single-proxy which is the best for all spectral periods. However, it is obvious that, regardless of the techniques used to derive amplification, T_0 has the best overall performance, especially for oscillator periods between 0.1 and 4.0 s. V_{S30} performs relatively well for periods from 0.2 to 0.7 s and is only second to T_0 in this period range, but for periods higher than 0.7 s, V_{S30} is among the worst-performing indexes. Site depth $Z_{0.8}$ exhibits nearly identical performance to T_0 at periods over 0.5 s, but site depth to a stiffer layer $Z_{1.0}$ does not further improve amplification estimation. Comparing the efficacies of V_{Sz} ($z = 5$, 10, 20 and 30 m), shear-wave velocity averaged to a larger depth can lead to better overall performance, and the improvement manifests in a period range from 0.2 to 0.7 s.

T_0 is shown to be the best-performing single-proxy among V_{Sz}, T_0, $Z_{0.8}$ and $Z_{1.0}$ in modelling linear site response at KiK-net sites. We then depict in Fig. 11a the σ_{Res1} reduction brought by replacing V_{S30} with T_0. Compared with the conventional parameter V_{S30}, using T_0 can reduce the site-to-site amplification variability by up to 17%, 24% and 27% for SSR_{PSA}, SSR_{FAS} and c-SSR_{FAS}, respectively. The reductions are negligible for spectral periods below 0.1 s, suggesting the inability of T_0 in improving amplification prediction in this range. There are troughs in the period range between 0.2 and 0.7 s (Fig. 11a) since V_{S30} performs relatively well at these periods, as shown in Fig. 11b which illustrates the Pearson correlation coefficient (R^2) between AF and V_{S30}. Fig 11b is nearly identical to Fig. 23 in the paper by Kawase and Matsuo (2004). At 0.1 s, AF scales poorly with V_{S30}, but at periods from 0.2 to 0.7 s, AF is well correlated with V_{S30}. Thus, for periods between 0.2 and 0.7 s, substituting T_0 for V_{S30} can only induce a limited reduction. The decrease in intersite variability is most pronounced at relatively long periods (>0.7 s), implying the efficiency of T_0 in this period band (Fig. 11a).

5 Site proxies (secondary) complementary to V_{S30} (primary)

It is known that V_{S30} alone cannot account for all aspects of site effects. However, given the widespread use of V_{S30} in current seismic provisions, replacing V_{S30} with a new site proxy appears to be unappealing for many. Considering that the V_{S30}-corrected residual amplification Res_1 shows a certain degree of dependency on T_0, as well as site depths $Z_{0.8}$ and $Z_{1.0}$, it is desirable to search for a site proxy complementary to V_{S30} in classifying a site or parameterizing site effects. Then the question arises as to which site index among T_0, $Z_{0.8}$ and $Z_{1.0}$ is the best parameter secondary to V_{S30} in modelling the residual amplification. To address this issue, we first model Res_1 as a quadratic function

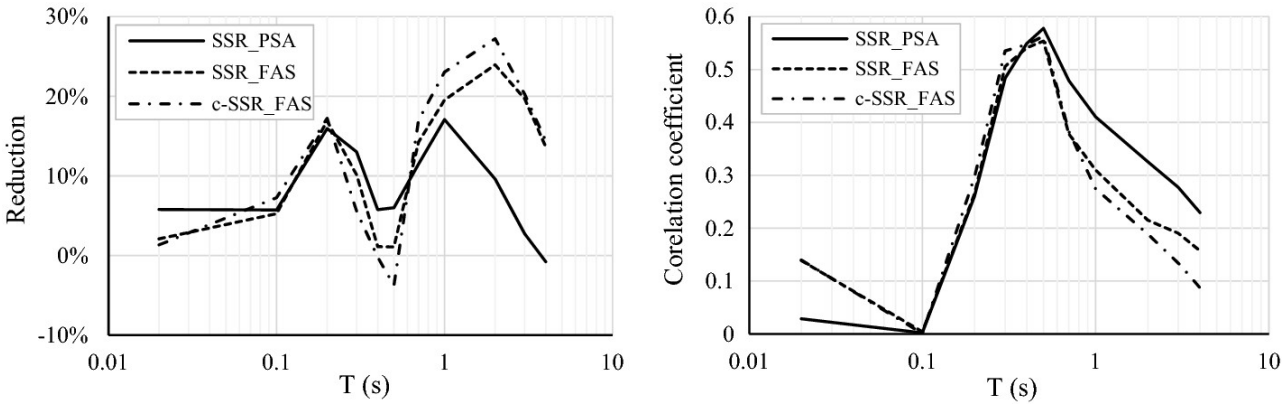

Figure 11. *(**a**) Reduction in intersite variability of model AF (T_0) relative to model AF (V_{S30}); (**b**) Pearson correlation coefficient between AF and V_{S30}.*

(Eq. 10) of a secondary site proxy (Y), including T_0, $Z_{0.8}$ and $Z_{1.0}$. Then we derive the residual Res_2 (Eq. 11) between Res_1 and proxy-based prediction $Res_1(Y)$, as well as its standard deviation σ_{Res2} (Eq. 12). The difference between σ_{Res1} and σ_{Res2} is then utilized to gauge the efficacy of each secondary site proxy. The best-performing candidate is considered to be the one that can produce the largest reduction.

$$Res_1(Y) = b_0 + b_1 \ln(Y) + b_2[\ln(Y)]^2 \tag{10}$$

$$Res_2 = Res_1 - Res_2(Y) \tag{11}$$

$$\sigma_{Res2} = \sqrt{\frac{\sum_1^N \left(Res_1 - Res_1(Y)\right)^2}{N}} \tag{12}$$

Figure 12 depicts the standard deviation (Eq. 12) and its relative reduction brought by adding an additional site proxy (secondary) on top of V_{S30} (primary). It shows that, for the investigated oscillator periods, all secondary parameters (T_0, $Z_{0.8}$ and $Z_{1.0}$) can reduce intersite amplification variability to different extents. At periods around 0.4 s, adding a secondary parameter into $AF(V_{S30})$ leads to a very limited reduction in variability. This is because, at periods around 0.4 s, V_{S30} performs well (Fig. 11b), and thus introducing an extra predictor variable can only induce an inconsequential improvement. However, for periods between 0.7 and 2.0 s, these additional variables are rather effective in improving amplification prediction.

The most remarkable reduction is achieved by T_0. The induced reductions are as much as 20% ($T = 1.0$ s), 27% ($T = 2.0$ s), and 26% ($T = 2.0$ s) for SSR$_{PSA}$, SSR$_{FAS}$ and c-SSR$_{FAS}$, respectively. T_0 is followed by $Z_{0.8}$, including which into the model $AF(V_{S30})$ leads to reductions up to 16% ($T = 1.0$ s), 17% ($T = 1.0$ s), and 15% ($T = 0.7$ s) for SSR$_{PSA}$, SSR$_{FAS}$ and c-SSR$_{FAS}$, respectively. In general, $Z_{1.0}$ is more difficult to obtain than $Z_{0.8}$, but the former does not instigate a more apparent reduction in site-to-site variability than the latter (Fig. 12). The percentages of decrease pertaining to $Z_{1.0}$ are 12% ($T = 1.0$ s), 17% ($T = 2.0$ s), and 15% ($T = 2.0$ s) for SSR$_{PSA}$, SSR$_{FAS}$ and c-SSR$_{FAS}$, respectively.

A three-dimensional (3D) subsurface velocity structure model, the Japan Seismic Hazard Information Station (J-SHIS) model, was constructed by Fujiwara et al. (2009) for the whole Japan (see Data and Resources). Regional velocity models are also available for some areas outside Japan, i.e., the 3D Community Velocity Model CVM-S4 (Kohler et al. 2003) and CVM-H1.1.0 (Süss and Shaw 2003) for the Southern California, as well as the 3D Velocity Model of the Bay Area (Boatwright et al. 2004) for the Northern California. These regional velocity models are developed primarily to model the propagation of long-period ground motions ($> \sim 1.0$ s). However, it is tempting to extract site parameters from these existing velocity models in a site-specific investigation. For instance, in the NGA-West2 project (Ancheta et al. 2014), subsurface models for Japan and California were queried to establish the site depth database. Thus, it is intriguing to examine to what extent the depth parameters extracted from a regional velocity model can improve site-response estimation if they are used as complementary proxies to V_{S30}.

We denote depths inferred from the J-SHIS model as Z_{x_infer} ($x = 0.8$, 1.0, 1.5 and 2.5 km/s). The subscript "infer" is to distinguish them from the measured depths. Following the same procedure as $Z_{0.8}$ and $Z_{1.0}$, we gauge the performances of Z_{x_infer} based on the decreases in site-to-site variability due to their incorporations into the amplification model $AF(V_{S30})$. Fig 13 displays the percentages of reduction in standard deviation. It can be seen that $Z_{0.8\_infer}$, $Z_{1.0\_infer}$, $Z_{1.5\_infer}$ and $Z_{2.5\_infer}$ can secure reductions, but the reductions do not exceed 8% ($T = 0.7$ s), 8% ($T = 0.7$ s), 10% ($T = 1.0$ s)

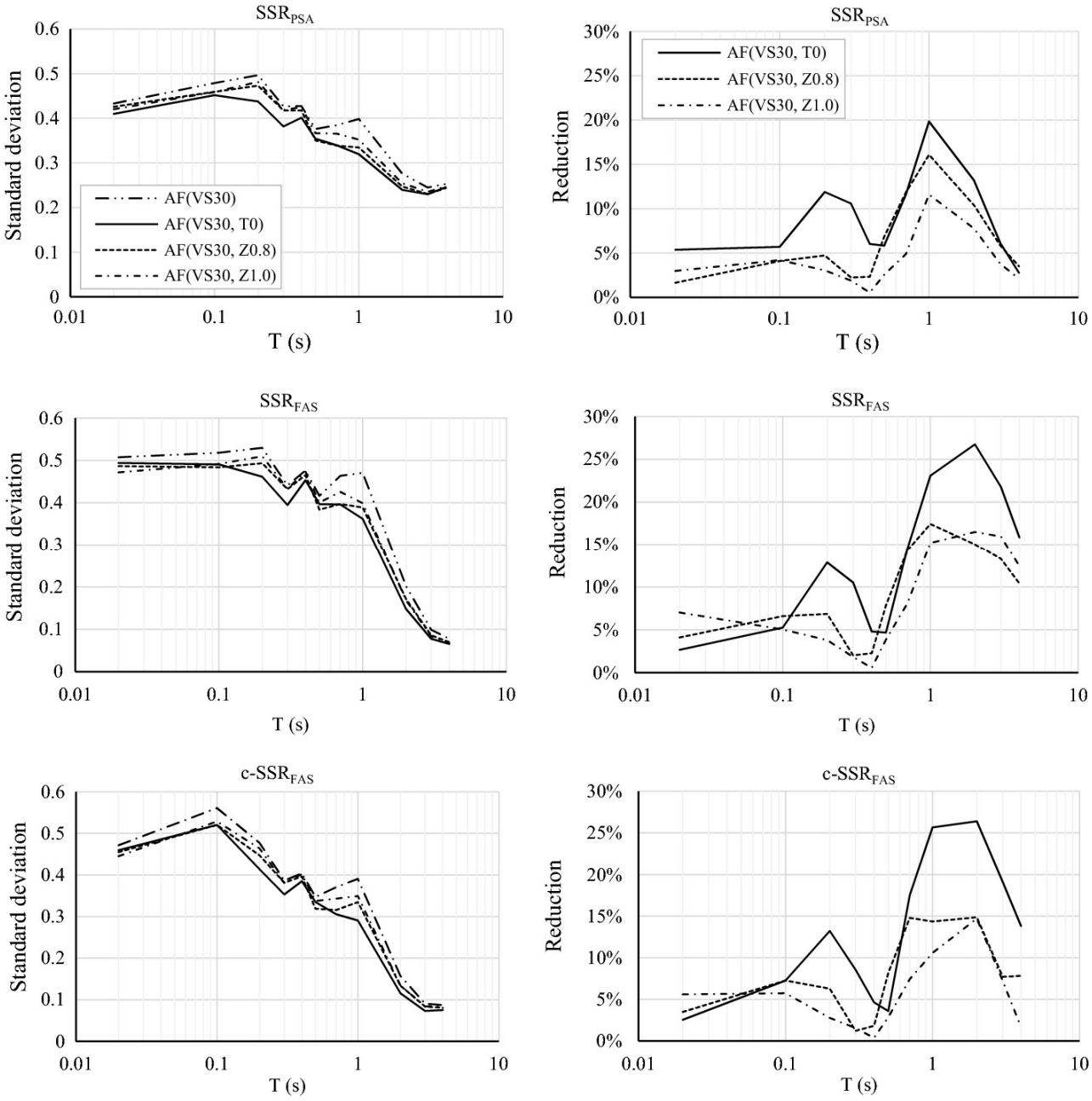

Figure 12. *Standard deviation of intersite amplification residuals (first column) of each amplification model and its relative reduction (second column) compared with that of model AF (V_{S30}) using SSR$_{PSA}$, SSR$_{FAS}$, and c-SSR$_{FAS}$.*

---

and 9% (T = 1.0 s), respectively. Comparing measured (Fig. 12) with inferred depths (Fig. 13), the formers ($Z_{0.8}$ and $Z_{1.0}$) are advantageous over their inferred counterparts ($Z_{0.8\_infer}$ and $Z_{1.0\_infer}$). This is mainly attributable to the different levels of uncertainty in inferred and measured depth data. Inferred depths from the J-SHIS model are biased and have a substantial amount of uncertainty when compared with site-specific depth measurements, as indicated by Zhu et al. (2019).

Although Z_{x_infer} (x = 0.8, 1.0, 1.5 and 2.5 km/s) perform less well than their measured counterparts, introducing Z_{x_infer} into $AF(V_{S30})$ can lead to a noticeable improvement in prediction. Thus, one can exploit an available regional velocity model for purposes other than long-period ground motion simulation. However, comparison with measured depths warrants a further improvement to the regional velocity model J-SHIS. As reported by Dhakal and Yamanaka (2013), there are evident

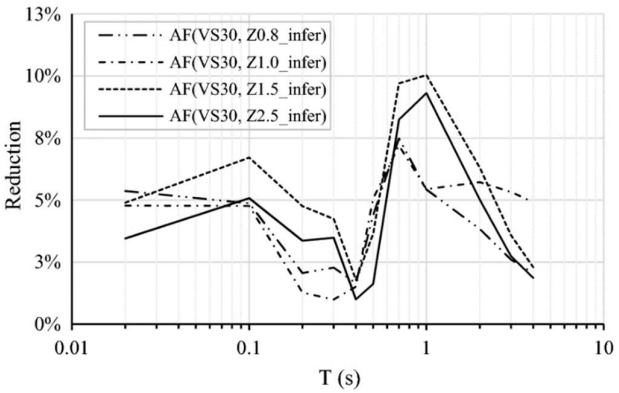

Figure 13. *Relative reduction in the standard deviation of intersite amplification residual due to the incorporation of inferred site depth Z_{x_infer} (x = 0.8, 1.0, 1.5 and 2.5 km/s) compared to model $AF(V_{S30})$ using SSR_{FAS}.*

discrepancies between the J-SHIS model and other subsurface models for the same region. For regions outside Japan, the 3D Community Velocity Model CVM (Version 2, Magistrale et al. 2000) for southern California was also found to have a significant bias (Stewart et al. 2005) and, as pointed out by Graves and Aagaard (2011), further refinement to the CVM was needed.

6 Site amplification as a function of T_0 (primary) and V_{Sz} (secondary)

In engineering practice, V_{S3} has already been derived at many recording stations and is widely adopted to categorize sites in current seismic codes (e.g., European code EC8) or to describe site effects in many GMMs (e.g., NGA-West2 GMMs). However, V_{S30} entails higher costs than T_0 which can be readily acquired using the *HVSR* technique on either ambient noises (Nakamura 1989) or earthquake recordings (Lermo and Chávez-García 1993). More importantly, T_0 is proved to be the best-performing single-proxy (Fig. 10) among V_{Sz}, T_0, $Z_{0.8}$ and $Z_{1.0}$ in depicting linear site effects. Thus, considering both the performance and engineering utility of T_0, as well as the established status of V_{Sz}, especially V_{S3} , we parameterize site effects using both parameters with T_0 as the primary and V_{Sz} as the secondary site indicator.

Figure 14 shows the site-to-site variabilities of each site-effect model, including $AF(T_0)$ and $AF(T_0, V_{Sz})$, as well as the percentages of reduction in variability due to the incorporation of V_{Sz} into $AF(T_0)$. Adding V_{Sz} as secondary site proxies can decrease estimation uncertainty. The reductions brought by V_{S5} and V_{S10} are insignificant, but the reduction increases with z (z = 5, 10, 20 and 30 m). V_{S2} and V_{S30} can lead to apparent variability reduction in the period range from 0.2 to 0.7 s, suggesting that, besides V_{S3} (Fig. 11b), V_{S20} performs also well in describing linear amplification in this period range. In comparison, the reduction as a result of the inclusion of V_{S30} into $AF(T_0)$ is less significant than the reduction due to the incorporation of T_0 into $AF(V_{S30})$ (Fig. 12), manifesting that T_0 alone can account for most of the site effects.

Figure 15a compares the intersite variabilities of the amplification (SSR_{PSA}) model $AF(T_0, V_{S30})$ with that of the model $AF(V_{S30}, T_0)$. The former uses T_0 as the primary and V_{S30} as the secondary predictor whereas the latter utilizes V_{S3} as the primary and T_0 as the secondary variable. The level of estimation uncertainty associated with $AF(T_0, V_{S30})$ is lower than that of $AF(V_{S30}, T_0)$, implying that the sequence of predictors entering the model affects the model efficacy. If both T_0 and V_{S30} were to be included in an amplification model, using T_0 as the primary indicator is preferable than the other way around, which is consistent with the finding of Hassani and Atkinson (2018a). Comparing with the configuration of V_{S3} (primary) and T_0 (secondary), Fig. 15b shows that the combination of T_0 (primary) and V_{S30} (secondary) can reduce model uncertainty by up to 12% (SSR_{PSA}), 7% (SSR_{FAS}) and 12% (c-SSR_{FAS}).

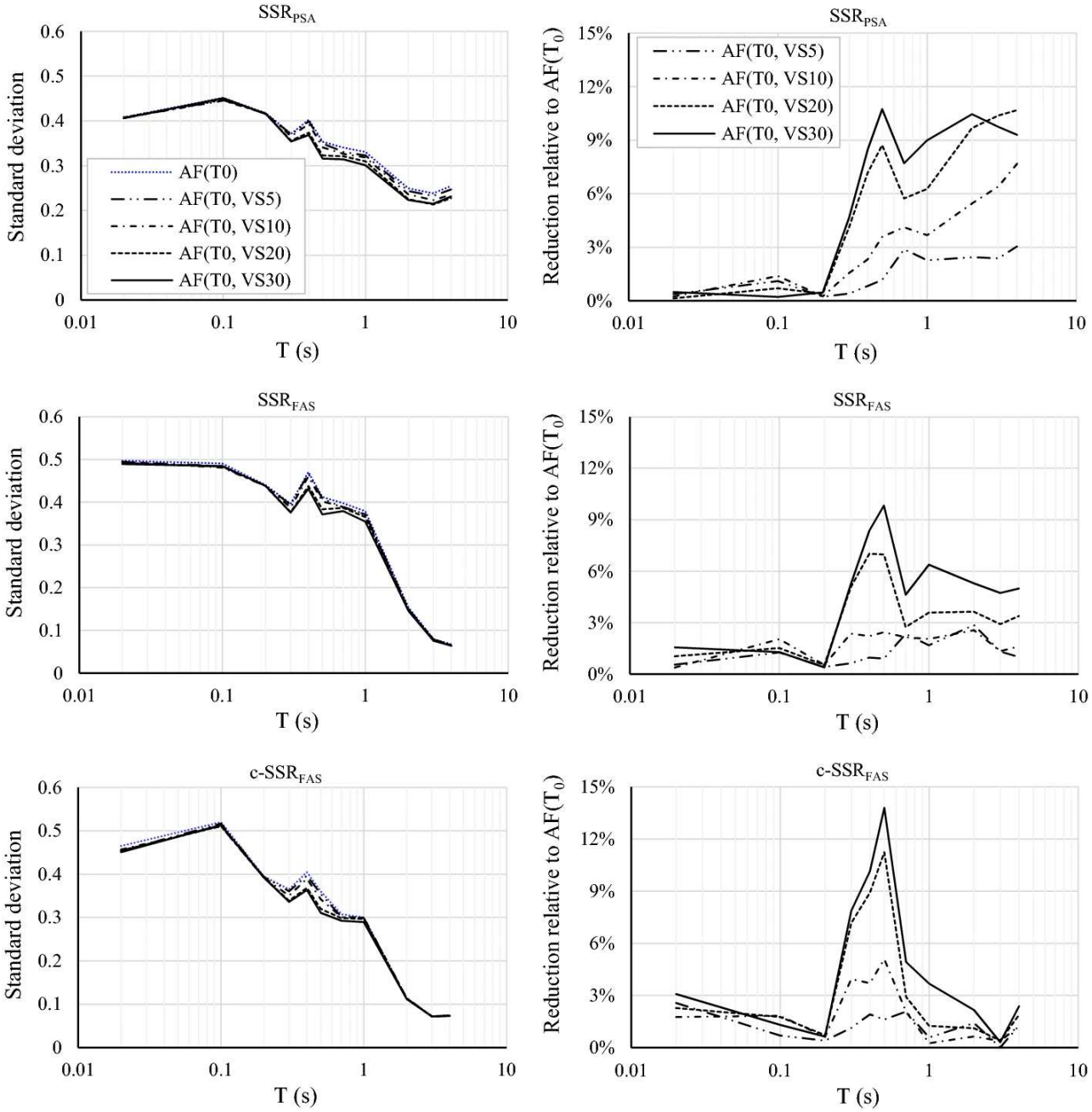

Figure 14. *Standard deviations of residuals of site-effects models using T_0 as the primary site proxy with or without V_{Sz} as the secondary predictor (left column); and relative reductions in the standard deviation of residuals of models $AF(T_0, V_{S5})$, $AF(T_0, V_{S10})$, $AF(T_0, V_{S20})$, and $AF(T_0, V_{S30})$ compared with $AF(T_0)$ (right column).*

7 Discussion and conclusions

In an effort to pinpoint the best-performing site proxy or optimal combination of site proxies in modelling linear site response, we selected 1840 ground-motion recordings from a KiK-net database processed by Dawood et al. (2016). Site effects were estimated using surface-to-borehole spectral ratios. T_0 was found to be the best-performing single-proxy among V_{Sz} ($z = 5$, 10, 20 and 30 m), T_0, $Z_{0.8}$ and $Z_{1.0}$. Substituting T_0 for V_{S3} in an amplification model could induce a significant reduction in site-to-site amplification variability, especially for spectral periods at 0.7 s or longer. There seems to be a consensus that T_0 has a better overall performance than V_{S30} in parameterizing site effects (e.g., Zhao

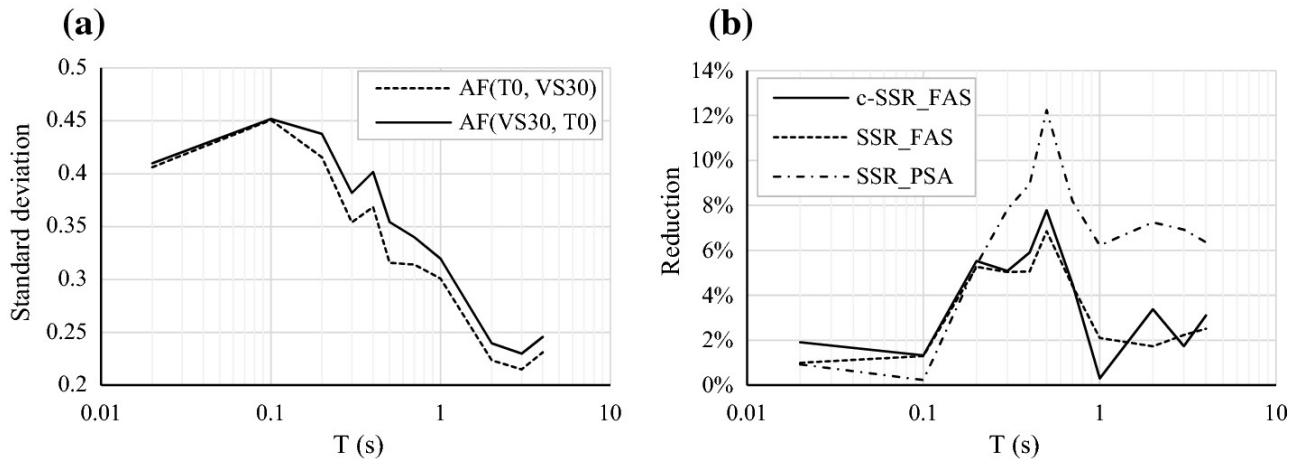

Figure 15. *(**a**) Standard deviations of residuals of amplification models of $AF(T_0, V_{S30})$ and $AF(V_{S30}, T_0)$ using SSR_{PSA}; (**b**) reduction in the uncertainty of model $AF(T_0, V_{S30})$ relative to model $AF(V_{S3}, T_0)$.*

---

and Xu 2013; Cadet et al. 2012; McVerry 2011; Derras et al. 2017; Stambouli et al. 2017; Hassani and Atkinson 2018a). T_0 is also recommended as one of the main proxies in the draft of revised EC8.

Besides, T_0 was also found in this study to be most descriptive of the residual amplification after V_{S30}-correction among T_0, $Z_{0.8}$, $Z_{1.0}$ and Z_{x_infer} (x = 0.8, 1.0, 1.5 and 2.5 km/s). In addition to V_{S30} (primary), adding T_0 (secondary) into an amplification model could reduce site-to-site amplification variability by up to 20–27% at relatively long periods (> 0.7 s). In site classification, Luzi et al. (2011) also achieved a significant reduction in variability when T_0 was included as a complimentary proxy to V_{S30}. This suggests that T_0 can be incorporated into current site-response models (or site terms) and site classification schemes to better account for site effects.

When T_0 was used as the primary proxy to model site response, T_0 alone could capture most of the site effects. Adding V_{S5} or V_{S1} (secondary) could only introduce a very limited further reduction in intersite amplification variability. In contrast, incorporating V_{S2} or V_{S3} (secondary) could apparently decrease variability at periods between 0.2 and 0.7 s but by no more than 10% and 14%, respectively. Furthermore, using T_0 as the primary and V_{S30} as the secondary predictor variables is better than the configuration of V_{S30} (primary) and T_0 (secondary), which confirms the results of Hassani and Atkinson (2018a).

Figure 16 compares the reductions in standard deviations of residuals between amplification observations and T_0-based predictions relative to the conventional model $AF(V_{S3})$. These relative reductions are given in Table 2. All T_0-based amplification models have less amount of uncertainty than $AF(V_{S3})$, especially for periods over 0.7 s. Adding V_{S10}, V_{S20} or V_{S3} into the model $AF(T_0)$ can further improve model performance, especially for spectral periods between 0.2 and 0.7 s. Although models $AF(T_0, V_{S30})$ and $AF(V_{S30}, T_0)$ utilize the same site proxies, the former performs better than the latter due to the difference in the sequence of variables entering the model. For the same reason, at least comparable overall performance to $AF(V_{S30}, T_0)$. Figure 16 also demonstrates that $AF(T_0, V_{S3})$ is the best-performing proxy pair but is only slightly better than $AF(T_0, V_{S20})$. Given that V_{S20} is strongly correlated with V_{S30} (e.g., Boore et al. 2011) and that V_{S30} may entail higher costs than V_{S2}, thus V_{S20} (secondary) may be adequate for engineering use.

T_0 is shown to be preferable in site characterization. However, our previous study (Zhu et al. 2019) found that there were discrepancies in T_0 derived using the *HVSR* technique by different teams. For sites with prominent 2D or 3D features, *HVSR* is not always reliable in determining T_0 (Gueguen et al. 2007). This may be one source of uncertainty in T_0 and will inevitably affect its efficacy. Besides, T_0

Table 2

Relative reductions in the standard deviation of residuals compared with *AF*(*VS*30)

Method	Model	T (s)											
		0.02 (%)	0.1 (%)	0.2 (%)	0.3 (%)	0.4 (%)	0.5 (%)	0.7 (%)	1 (%)	2 (%)	3 (%)	4 (%)	Ave.
SSRPSA	$AF(V_{S30}, T_0)$	5	6	12	11	6	6	12	20	13	6	3	9
	$AF(T_0)$	6	6	16	13	6	6	11	17	10	3	−1	8
	$AF(T_0, V_{S10})$	6	7	16	14	8	9	15	20	15	9	7	12
	$AF(T_0, V_{S20})$	6	6	16	17	13	14	17	22	18	13	10	14
	$AF(T_0, V_{S30})$	6	6	16	17	14	16	18	25	19	12	9	14
SSRFAS	$AF(V_{S30}, T_0)$	3	5	13	11	5	5	15	23	27	22	16	13
	$AF(T_0)$	2	5	17	10	1	1	14	20	24	20	14	12
	$AF(T_0, V_{S10})$	2	7	17	12	3	3	16	21	26	21	15	13
	$AF(T_0, V_{S20})$	3	7	17	15	8	8	17	22	27	22	17	15
	$AF(T_0, V_{S30})$	4	6	17	15	9	11	18	25	28	23	18	16
c-SSRFAS	$AF(V_{S30}, T_0)$	3	7	13	9	5	4	18	26	26	19	14	13
	$AF(T_0)$	1	7	17	6	0	−4	17	23	27	20	14	12
	$AF(T_0, V_{S10})$	3	9	18	9	3	2	19	23	28	21	15	14
	$AF(T_0, V_{S20})$	4	9	18	12	9	8	19	24	28	21	16	15
	$AF(T_0, V_{S30})$	4	8	18	13	10	11	21	26	29	21	16	16

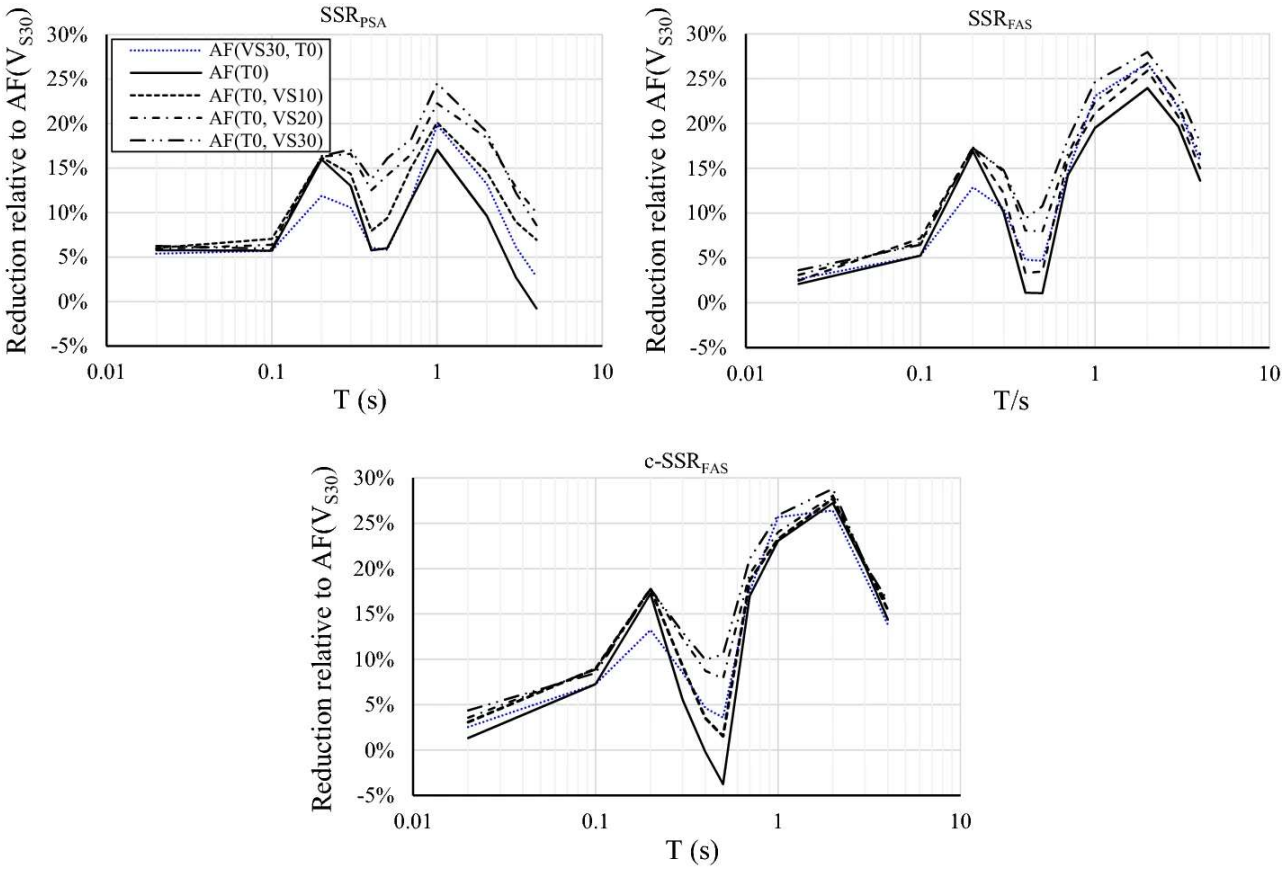

Figure 16. *Relative reductions in the standard deviation of residuals of models $AF(T_0)$, $AF(T_0, V_{S10})$, $AF(T_0, V_{S2})$, $AF(T_0, V_{S30})$ and $AF(V_{S30}, T_0)$ compared with $AF(V_{S30})$.*

is identified as corresponding to a significant peak on *HVSR*, but significant peaks are often defined rather subjectively, which may be another source of uncertainty in T_0. Thus, one should take due consideration of these factors when detecting T_0 using the *HVSR* method. In this study, we used only KiK-net sites which are often located on weathered rocks or thin sediments (Aoi et al. 2000). This is compatible with the maximum usable period of our selected recordings, i.e., at least 4.17 s since there are no prominent site effects beyond this period. However, there exist sites with rather thick sediments, especially those in deep sedimentary basins, e.g., the Kanto (Tokyo) basin in Japan and the Los Angeles basin in California. At these sites, there are significant amplifications at periods longer than 4.17 s. Also, basin-generated surface waves are likely to have a strong presence in the recordings. Thus, the best-performing site proxy or combination of proxies should be further tested on deep basin sites and in a broad period range preferably up to ~ 10.0 s. Meanwhile, it needs to be stressed that site amplifications in this research are referenced to downhole bedrocks with different velocities (larger than 800 m/s). Since all site proxies are gauged on the same dataset, inhomogeneous reference site conditions will not affect the results. However, amplification should be normalized to a common reference for the development of empirical prediction models. In addition, we limit our study to the linear domain, but soft soil sites exhibit nonlinear behavior during strong ground shakings. Thus, the efficiencies of various site parameters in depicting nonlinear site response need to be investigated in future studies.

What distinguishes this work from many preceding ones is that we include many competitive site proxies all in one study. In addition to V_{Sz} ($z = 5$, 10, 20 and 30 m) and T_0, we also consider various depth parameters with differentiation of measured ($Z_{0.8}$ and $Z_{1.0}$) from inferred depths (Z_{x_infer}, $x =$

0.8 and 1.0, 1.5 and 2.5 km/s). Though $Z_{1.5}$ and $Z_{2.5}$ are also candidate proxies utilized in some research, e.g., $Z_{1.5}$ in the amplification model by Choi et al. (2005) and $Z_{2.5}$ in the site term of Campbell and Bozorgnia (2014), we do not include them here since there are not adequate sites with measured $Z_{1.5}$ and $Z_{2.5}$ available. For instance, there are only 42 KiK-nets sites of which borehole drillings penetrate 2.5 km/s horizon.

In summary, our results show that T_0 is the best-performing single-proxy among V_{Sz}, T_0, $Z_{0.8}$ and $Z_{1.0}$ in modelling linear site response at KiK-net sites. Thus, T_0 can be used as a substitute for V_{S30}. Meanwhile, T_0 is also the best-performing proxy among T_0, $Z_{0.8}$, $Z_{1.0}$ and Z_{x_infer} complementary to V_{S30} in capturing the V_{S30}-corrected residual amplification. Hence, T_0 can be utilized as an add-on to calibrate existing V_{S30}-based amplification models or site terms. Besides, T_0 alone can capture most of the site effects and should be utilized as the primary site proxy. (T_0, V_{S30}) is found to be the best-performing proxy pair among (V_{S30}, T_0), ($V_{S30}, Z_{0.8}$), ($V_{S30}, Z_{1.0}$), (V_{S30}, Z_{x_infer}) and (T_0, V_{Sz}) but is only slightly better than $AF(T_0, V_{S2}$). Given that V_{S30} may entail higher costs than V_{S20}, the configuration of T_0 (primary) and V_{S20} (secondary) is considered to be the optimal combination.

Acknowledgements We are grateful to the National Research Institute for Earth Science and Disaster Prevention (NIED), Japan, for making the site data of KiK-net recording stations, as well as the J-SHIS velocity model easily accessible to the public. The first author thanks Dr. Haitham Dawood for providing the processed KiK-net dataset, and Prof. Yu Miao for providing KiK-net site-period data. This work is supported by the Seismology and Earthquake Engineering Research Infrastructure Alliance for Europe (SERA) project funded by the EU Horizon 2020 Programme under Grant Agreement Number 730900.

Data and Resources Velocity profiles of KiK-net recording stations were downloaded from the http://www.kyoshin.bosai.go.jp (last accessed on 05/06/2018). The J-SHIS velocity model was downloaded from http://www.j-shis.bosai.go.jp/map/?lang=en (last accessed on 05/06/2018).

References

Abrahamson NA, Youngs RR (1992) A stable algorithm for regression analyses using the random effects model. Bull Seismol Soc Am 82:505–510

Al Atik L, Abrahamson N, Bommer JJ, Scherbaum F, Cotton F, Kuehn N (2010) The variability of ground-motion prediction models and its components. Bull Seismol Soc Am 81:794–801

Ancheta TD, Darragh RB, Stewart JP, Seyhan E, Silva WJ, Chiou BSJ, Wooddell KE, Graves RW, Kottke AR, Boore DM, Kishida T, Donahue JL (2014) NGA-West2 database. Earthq Spectra 30:989–1005

Aoi S, Obara K, Hori S, Kasahara K, Okada Y (2000) New Japanese uphole/downhole strong-motion observation network: KiK-net. Seismol Res Lett 72:239

Assimaki D, Li W, Steidl JH, Tsuda K (2008) Site amplification and attenuation via downhole array seismogram inversion: a comparative study of the 2003 Miyagi-Oki aftershock sequence. Bull Seismol Soc Am 98:301–330

Atkinson GM, Boore DM (2003) Empirical ground-motion relations for subduction zone earthquakes and their application to Cascadia and other regions. Bull Seismol Soc Am 93:1703–1729

Bazzurro P, Cornell CA (2004) Ground-motion amplification in nonlinear soil sites with uncertain properties. Bull Seismol Soc Am 94:2090–2109

Bendat JS, Piersol AG (1980) Engineering applications of correlation and spectral analysis. Wiley, New York

Biggs JM (1964) Introduction to structural dynamics. McGraw-Hill, New York

Boatwright J, Blair L, Catchings R, Goldman M, Perosi F, Steedman C (2004) Using twelve years of USGS refraction lines to calibrate the Brocher and Others (1997) 3-D velocity model of the bay area. U.S. Geological Survey Open-File Report 2004-1282, Washington, D.C

Boore DM, Thompson E, Cadet H (2011) Regional correlations of VS30 and velocities averaged over depths less than and greater than 30 meters. Bull Seismol Soc Am 101:3046–3059

Boore DM, Stewart JP, Seyhan E, Atkinson GM (2014) NGA-West2 equations for predicting PGA, PGV, and 5% damped PSA for shallow crustal earthquakes. Earthq Spectra 30:1057–1085

Bora SS, Scherbaum F, Kuehn N, Stafford P (2016) On the relationship between fourier and response spectra: implications

for the adjustment of empirical ground-motion prediction equations (GMPEs). Bull Seismol Soc Am 106:1235–1253
Borcherdt RD (1994) Estimates of site-dependent response spectra for design (methodology and justification). Earthq Spectr 10:617–653
Cadet H (2007) Utilisation combinée des méthodes basées sur le bruit de fond dans le cadre du microzonage sismique. Ph.D. thesis, Joseph Fourier University (**in French**)
Cadet H, Bard P-Y, Rodriguez-Marek A (2012) Site effect assessment using KiK-net data: part 1. A simple correction procedure for surface/downhole spectral ratios. Bull Earth Eng 10:421–448
Campbell KW, Bozorgnia Y (2014) NGA-West2 ground motion model for the average horizontal components of PGA, PGV, and 5%-damped linear Response Spectra. Earthq Spectra 30:1087–1115
Choi Y, Stewart JP, Graves RW (2005) Empirical model for basin effects accounts for basin depth and source location. Bull Seismol Soc Am 95:1412–1427
Dawood HM, Rodriguez-Marek A, Bayless J, Goulet C, Thompson E (2016) A flatfile for the KiK-net database processed using an automated protocol. Earthq Spectra 32:1281–1302
Derras B, Bard P-Y, Cotton F (2017) *VS30*, slope, *H800* and *f0*: performance of various site-condition proxies in reducing ground-motion aleatory variability and predicting nonlinear site response. Earth Planets Space 69:133. https://doi.org/10.1186/s4062 3-017-0718-z
Dhakal YP, Yamanaka H (2013) An evaluation of 3-D velocity models of the Kanto basin for long-period ground motion simulations. J Seismol 17:1073–1102
Field EH, Jacob KH, Hough SE (1992) Earthquake site responses estimation: a weal-motion case study. Bull Seismol Soc Am 82:2283–2307
Fujimoto K, Midorikawa S (2006) Relationship between average shear-wave velocity and site amplification inferred from strong motion records at nearby station pairs. J Jpn Assoc Earthq Eng 6:11–22 **(in Japanese with English abstract)**
Fujiwara H, Kawai S, Aoi S, Morikawa N, Senna S, Kudo N, Ooi M, Hao KX, Hayakawa Y, Yoyama N, Matsuyama H, Iwamoto K, Suzuki H, Liu Y (2009) A study on subsurface structure model for deep sedimentary layers of Japan for strong-motion evaluation. Technical Note of the National Research Institute for Earth Science and Disaster Prevention, No. 337
Gallipoli MR, Mucciarelli M (2009) Comparison of site classification from VS30, VS10, and HVSR in Italy. Bull Seismol Soc Am 99:340–351
Graves RW, Aagaard BT (2011) Testing long-period ground-motion simulations of scenario earthquakes using the Mw 7.2 El Mayor-Cucapah mainshock: evaluation of finite-fault rupture characterization and 3D seismic velocity models. Bull Seismol Soc Am 101:895
Gueguen P, Cornou C, Garambois S, Banton J (2007) On the limitation of the H/v spectral ratio using seismic noise as an exploration tool: application to the Grenoble valley (France), a Small Apex Ratio Basin. Pure appl Geophys 164:115–134
Hassani B, Atkinson GM (2018a) Site-effects model for central and eastern North America based on peak frequency and average shear-wave velocity. Bull Seismol Soc Am 107:338–350
Hassani B, Atkinson GM (2018b) Application of a site-effects model based on peak frequency and average shear-wave velocity to California. Bull Seismol Soc Am 108:351–357
Japan Road Association (1990) Specifications for highway bridges part V, Seismic Design, Maruzen Co., Ltd.
Kawase H, Matsuo H (2004) Amplification characteristics of K-NET, KiK-net, and JMA Shindokei network sites based on the spectral inversion technique. In: 13th world conference on earthquake engineering, Vancouver, Canada
Kohler M, Magistrale H, Clayton R (2003) Mantle heterogeneities and the SCEC three-dimensional seismic velocity model version 3. Bull Seismol Soc Am 93:757–774
Konno K, Ohmachi T (1998) Ground-motion characteristics estimated from spectral ratio between horizontal and vertical components of microtremor. Bull Seismol Soc Am 88:228–241
Kotha SR, Cotton F, Bindi D (2018) A new approach to site classification: mixed-effects ground motion prediction equation with spectral clustering of site amplification functions. Soil Dyn Earthq Eng 110:318–329
Lermo J, Chávez-García FJ (1993) Site effect evaluation using spectral ratios with only one station. Bull Seismol Soc Am 83:1574–1594
Luzi L, Puglia R, Pacor F, Gallipoli MR, Bindi D, Mucciarelli M (2011) Proposal for a soil classification based on parameters alternative or complementary to Vs, 30. Bull Earthq Eng 9:1877–1898
Magistrale H, Day S, Clayton R, Graves RW (2000) The SCEC Southern California reference three-dimensional seismic velocity model version 2. Bull Seismol Soc Am 90: S65–S76
McVerry GH (2011) Site-effect terms as continuous functions of site period and Vs30. In: Pacific conference on earthquake engineering: building an earthquake resilient society, Auckland, New Zealand
Nakamura Y (1989) A method for dynamic characteristics estimation of subsurface using microtremor on the ground surface. Quarterly Report of Railway Technical Research Institute (RTRI), vol. 30, no 1
Okada Y, Kasahara K, Hori S, Obara K, Sekiguchi S, Fujiwara H, Yamamoto A (2004) Recent progress of seismic observation

networks in Japan-Hi-net, F-net, K-NET and KiK-net. Earth Planets Space 56:15–28
Oth A, Bindi D, Parolai S, Di Giacomo D (2011) Spectral analysis of K-NET and KiK-net data in Japan, part II: on attenuation characteristics, source spectra, and site response of borehole and surface stations. Bull Seismol Soc Am 101:667–687
Pilz M, Cotton F (2019) Does the 1D assumption hold for site response analysis? A study of seismic site responses and implication for ground motion assessment using KiK-net strong-motion data. Earthq Spectra 35:883–905
Pitilakis K, Gazepis C, Anastasiadis A (2004) Design response spectra and soil classification for seismic code provisions. In: Proceedings of the 13th world conference on earthquake engineering, Vancouver, B.C., Canada
Pitilakis K, Riga E, Anastasiadis A (2013) New code site classification, amplification factors and normalized response spectra based on a worldwide ground-motion database. Bull Earthq Eng 11:925–966
Pitilakis K, Riga E, Anastasiadis A, Fotopoulou S, Karafagka S (2018) Towards the revision of EC8: proposal for an alternative site classification scheme and associated intensity dependent spectral amplification factors. Soil Dyn Earthq Eng. https ://doi.org/10.1016/j.soild yn.2018.03.030
Régnier J, Bonilla LF, Bertrand E, Semblat JF (2014) Influence of the VS profiles beyond 30 m depth on linear site effects: assessment from the KiK-Net data. Bull Seismol Soc Am 104:2337–2348
Şafak E (1997) Models and methods to characterize site amplification from a pair of records. Earhq Spectra 13:97–129
Shearer PM, Orcutt JA (1987) Surface and near-surface effects on seismic waves: theory and borehole seismometer results. Bull Seismol Soc Am 77:1168–1196
Si H, Midoriakwa S (1999) New attenuation relationships for peak ground acceleration and velocity considering effects of fault type and site condition. J Struct Constr Eng (Trans AIJ) 523:63–70 **(in Japanese with English abstract)**
Stafford PJ, Rodriguez-Marek A, Edwards B, Kruiver PP, Bommer JJ (2017) Scenario dependence of linear site-effect factors for short-period response spectral ordinates. Bull Seismol Soc Am 107:2859–2872
Stambouli AB, Zendagui D, Bard PY, Derras B (2017) Deriving amplification factors from simple site parameters using generalized regression neural networks: implications for relevant site proxies. Earth Planets Space 69:99. https://doi.org/10.1186/s4062 3-017-0686-3
Steidl JH (1993) Variation of site response at the UCSB dense array of portable accelerometers. Earthq Spectra 9:289–302
Stewart JP, Choi Y, Graves RW, Shaw JH (2005) Uncertainty of Southern California basin depth parameters. Bull Seismol Soc Am 95:1988–1993
Süss MP, Shaw JH (2003) P wave seismic velocity structure derived from sonic logs and industry reflection data in the Los Angeles basin, California, J Geophys Res Solid Earth 108(B3): Article no 2170
Thompson EM, Baise LG, Kayen RE, Guzina BB (2009) Impediments to predicting site response: seismic property estimation and modeling simplifications. Bull Seismol Soc Am 99:2927–2949
Van Houtte C, Drouet S, Cotton F (2011) Analysis of the origins of κ (Kappa) to compute hard rock to rock adjustment factors for GMPEs. Bull Seismol Soc Am 101:2926–2941
Wang SY, Shi Y, Jiang WP, Yao EL, Miao Y (2018) Estimating site fundamental period from shear-wave velocity profile. Bull Seismol Soc Am 108:3431–3445
Welch PD (1967) The use of fast Fourier transforms for the estimation of power spectra: a method based on time averaging over short modified periodograms. IEEE Trans Audio Electroacoust 15:70–73
Zhao JX, Xu H (2013) A comparison of VS30 and site period as site-effect parameters in response spectral ground-motion prediction equations. Bull Seismol Soc Am 103:1–18
Zhao JX, Irikura K, Zhang J, Fukushima Y, Somerville PG, Asano A, Ohno Y, Oouchi T, Takahashi T, Ogawa H (2006) An empirical site classification method for strong motion stations in Japan using H/V response spectrum ratio. Bull Seismol Soc Am 96:914–925
Zhu C, Cotton F, Pilz M (2019) Testing the depths to 1.0 and 2.5 km/s velocity isosurfaces in a velocity model for Japan and implications for ground-motion modeling. Bull Seismol Soc Am. https ://doi.org/10.1785/01201 90016

Affiliations

Chuanbin Zhu[1] · Marco Pilz[1] · Fabrice Cotton[1,2]

[1] GFZ German Research Centre for Geosciences, Telegrafenberg, 14473 Potsdam, Germany
[2] University of Potsdam, Institute for Earth Sciences, Karl-Liebknecht-Str. 24-25, 14476 Potsdam, Germany